THE EFFECTS OF TRAUMATIC BRAIN INJURY ON NEOCORTICAL SEROTONIN AXON INNERVATION

by
Tymoteusz Jan Kajstura

A dissertation submitted to Johns Hopkins University in conformity with the requirements for the degree of Doctor of Philosophy in Neuroscience.

Baltimore, MD

August 2016

Abstract

It is widely held that injured neurons in the central nervous system do not have the capacity to undergo axonal regeneration. Recently, however, there is mounting evidence that serotonin fibers are an exception to this rule. Serotonin fibers undergo long-distance regeneration in the neocortex after amphetamine lesion. They can also traverse the rift created by a penetrating injury in the neocortex. These new fibers are indistinguishable in morphology from spared axons and have been shown to be competent to release serotonin. While experimentally useful, these models do not mimic the most typical clinical injuries. Traumatic brain injury (TBI) is prevalent and can lead to pathologies such as depression that are a result of serotoninergic dysfunction. So whether serotonin fibers can regrow after TBI is an important question. To address this, we used a controlled cortical impact (CCI) model to evoke injury in adult mouse neocortex and assessed serotonin fiber innervation one week, one month, and three months after injury with immunohistochemistry. In the neocortex serotonin fibers traverse in an anterior to posterior direction. CCI, as well as an open skull injury without impact, resulted in decreases in serotonin fiber innervation posterior to the injury site one week after surgery. At one month and three months after surgery there was a significant regrowth of serotonin fibers posterior to the injury. We also quantified reactive astrocytes following TBI using GFAP immunohistochemistry. There was profound reactive astrogliosis one week after surgery that decreased close to control levels by three months. Interestingly, the amount of reactive gliosis was not correlated to the amount of serotonin fiber loss in

either regions anterior or posterior to the injury. Microglial density was not affected by TBI. In addition, we investigated whether a repetitive mild TBI model leads to serotonin fiber loss in mouse neocortex. We did not detect serotonin fiber loss across a range of injury severities despite the presence of reactive gliosis in the optic fiber tract accompanying these injuries. These findings indicate that serotonin fibers can be damaged in certain clinically relevant TBI models and are capable of regrowth following injury.

Thesis committee:

David Linden, Ph.D. (advisor, first reader)

Dwight Bergles, Ph.D. (chair)

Solange Brown, M.D., Ph.D. (second reader)

Elisabeth Glowatzki, Ph.D.

Acknowledgements

I owe a great to deal of gratitude to everyone who has provided guidance, support, and assistance in the completion of this dissertation. First, to my advisor Dr. David Linden. Without his patience, motivation, wisdom, and advice this project would not have been possible. His tendency to pop out of his office with weird scientific facts also kept the process entertaining. To the rest of my thesis committee – Drs. Bergles, Brown, and Glowatzki. Their feedback on this project was invaluable and they were instrumental in helping guide me towards success. To the rest of the Linden Lab, especially Drs. Sarah Dougherty and Yunju Jin. Their projects were the groundwork for this dissertation and they were always more than willing to lend their technical expertise, ideas, and support. I am grateful to have gotten to add a piece to the story they started. To Drs. Xu and Koliatsos for their assistance with the repetitive mild traumatic brain injury portion of the project. To the administrative staff in the Department of Neuroscience as well as the MD/PhD Program. They have always kept me on track and made me feel like part of the Hopkins family. To Dr. Michele Pucak, who made using the Multiphoton Core Facility a pleasure and kept everything up and running. To my parents, who always made sure I was happy, healthy, and well fed. And working hard. Last, and most important, to my fiancée Dr. Ellen Ambrose. It is no exaggeration to say that this dissertation wouldn't have come to fruition without her constant support. She never let me give up, was always able to provide new insights, and inspired me with her own work on a daily basis. For everything, thank you.

Table of contents

List of Tables

List of Figures

Chapter 1: Background

Serotonin is a monoamine neurotransmitter with biological roles ranging from early development through the lifespan (Muller and Jacobs, 2010). Diverse receptors for serotonin are ubiquitous in the adult mammalian brain, explaining how serotonin can be involved in behaviors including, but not limited to, thermal regulation, feeding, sexual behavior, aggression, stress, response to pain, and mood (Lucki, 1998). Serotonin is synthesized in two steps from its precursor tryptophan, and is released both at synaptic contacts and via paracrine or volume transmission. In the cortex, volume transmission vastly dominates over synaptic transmission. Electron microscopy studies have revealed that the majority of bouton structures on serotonin fibers do not make post-synaptic contacts either on the dendrites or somata of neocortical neurons across a range of species (Beaudet and Descarries, 1978; DeFelipe and Jones, 1988; Horung, 2003). Concentration of serotonin in the milieu is in large part regulated by reuptake by the serotonin transporter SERT (Murphy and Lesch, 2008).

There are seven families of serotonin receptors, named 5-$HT_{1\text{-}7}$. With the exception of 5-HT_3, which is a ligand gated cation channel, serotonin receptors are G-protein coupled (Murphy et al., 1998). The subtypes of the largest receptor family, 5-HT_1, are linked to $G_{i/o}$ and inhibit cyclic adenosine monophosphate (cAMP) production leading to inhibitory effects. Subtypes of the 5-HT_5 family also appear to couple to $G_{i/o}$ (Nelson, 2004). Receptors

5-HT_4, 5-HT_6, and 5-HT_7, are primarily coupled to G_s effector proteins, increase cAMP production, and are generally excitatory. The 5-HT_2 family effector molecules are the $G_{q/11}$ subunit, which activate phospholipase C. While evidence suggests that these receptor families have overlapping and diverse physiological roles, behavioral and pharmacological data suggest that 5-HT_{1A}, 5-HT_{1B}, and 5-HT_{2A} receptors play the largest role in clinically relevant mood disorders (Fakhoury, 2016).

Serotonin system in mice

Nearly every structure in the brain receives serotonin fiber innervation. The serotonergic system in mice is divided into two distinct groups of neurons in the midbrain. The rostral group contains cell bodies that send projections to the forebrain while the caudal group of cell bodies sends projections to hindbrain and spinal cord (Figure 1; Tork, 1990). The caudal group includes the raphe magnus nucleus, raphe pallidus nucleus, and raphe obscurus, which all project to the spinal cord as well as the medullary reticular formation nuclei which have axonal projections that innervate the cerebellum (Manto et al., 2013).

The rostral division contains the dorsal raphe nucleus and median raphe nucleus. Both of these nuclei have extensive ascending axons that follow a C-shaped projection through the lateral hypothalamus and basal forebrain in a dense path termed the medial forebrain bundle. The fibers then turn dorsally at the frontal cortex before turning posteriorly to continue through the parietal, occipital, and temporal cortex. Along the way axons branch

to innervate many forebrain structures including the hypothalamus, thalamus, amygdala, accumbens, striatum, and the olfactory bulbs. In the neocortex, fibers originating from the median raphe preferentially innervate layer 1 while fibers from the dorsal raphe preferentially innervate deeper layers (Vitalis et al., 2013). Along with different innervation patterns, the fibers from the median and dorsal raphe nuclei differ morphologically. Axons originating in the dorsal raphe are thin, branch profusely, and have small boutons. These fibers are not likely to form synaptic contacts. In contrast, fibers from the median raphe have large round boutons that have been shown with electron microscopy to form synaptic contacts on cell bodies and dendrites of their postsynaptic targets (Tork, 1990; Wilson and Molliver, 1994).

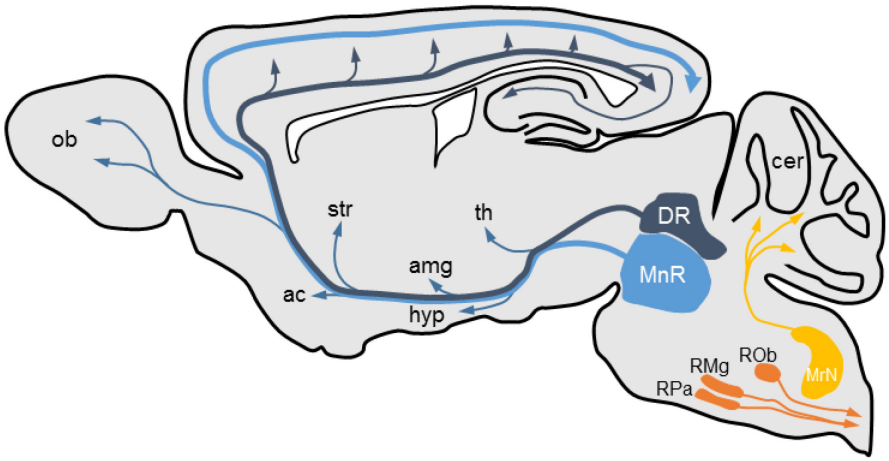

Figure 1. Serotonin fiber innervation of the adult mouse brain. Serotonin cell bodies are located in brainstem nuclei and their axons project throughout the central nervous system innervating regions including the neocortex, nucleus accumbens (ac), amygdala (amg),

cerebellum (cer), hypothalamus (hyp), olfactory bulb (ob), striatum (str), and thalamus (th). DR = dorsal raphe, MnR = median raphe, MrN = medullary reticular nuclei, RMg = raphe magnus, ROb = raphe obscurus, RPa = raphe pallidus.

Regenerative capacity of serotonin fibers

It is widely held that injured neurons in the central nervous system do not have the capacity to regenerate axons (Tuszynski and Steward, 2012). While there have been reports of rewiring in the neocortex following laser ablation of axons from excitatory, glutamatergic neurons, regrowth is rare (Canty et al., 2013). Regrowth into or through an injured area can take one of two distinct forms, which are not mutually exclusive. Regrowth from a transected or injured axon itself, whether directly from the severed end or proximal to it, is considered regeneration. Meanwhile, growth from non-damaged axons to compensate for innervation loss from damaged axons is termed local sprouting rather than regeneration (Tuszynski and Steward, 2012).

One reason that regrowth is rare following injury rests on the fact that damaged tissue is not a permissive environment for axonal growth. Myelin debris within the damaged region expresses several inhibitory molecules including Nogo-A. The Nogo-66 domain of Nogo-A acts on the Nogo-A receptor NgR to cause axonal growth cone collapse (Fournier et al., 2001). Extracellular matrix molecules secreted by support cells responding

to the injury can also inhibit growth in the damaged area. Reactive astrocytes have been shown to secrete chondroitin sulfate proteogylcans (CSPGs) which contain linear disaccharide chains that act as a stop signals and serve to hinder axonal growth (Bovolenta et al., 1993). In addition to these stop signals, chemorepellent molecules such as Slit are also expressed at the injury site preventing growth of axons into the area (Hagino et al., 2003).

Limited rewiring due to local sprouting or regeneration from damaged ends is suggestive of the fact that neurons can retain some intrinsic capacity to regrow axons. Not all cell types appear to have the capacity to rewire locally, however, even in a permissive environment. Indeed, recent studies are beginning to converge on the conclusion that diminished intrinsic regenerative capacity in mature neurons is a major factor limiting regeneration (Sun and He, 2010). Intrinsic regenerative capacity is likely to have many determinants. These include, but may not be limited to, expression of receptors for stop signals, retrograde transport of injury signals to the nucleus from the site of axonal injury, and the transcriptional and translational machinery necessary to induce a growth program (Zou et al., 2009).

There is mounting evidence that serotonin neurons have an unusually potent intrinsic capacity for axonal regeneration. Following cervical spine injury serotonin fibers were found to regenerate into a peripheral nerve graft that was treated with chondroitinase

ABC (ChABC) to break down the inhibitory disaccharide chains on CSGPs (Alilain et al., 2011). Twelve weeks after spinal cord injury and peripheral nerve graft, serial reconstruction, retrograde viral tracers, and immunohistochemistry showed that serotonin fibers had regenerated from brainstem nuclei, into the graft, and further into spinal cord. This regeneration was accompanied by restoration of diaphragmatic function. More distal spinal cord injuries have revealed that serotonin fiber regeneration isn't limited by proximity to the brainstem raphe nuclei (Lee et al., 2013). Following a complete thoracic spinal cord transection, mice were treated with a peripheral nerve graft treated with ChABC and a fibroblast growth factor. Six months after injury and graft, there was regeneration of serotonin fibers. While the majority terminated either in the graft or within 250 μm into the lesion site, some fibers were observed as distal as 12 mm beyond the lesion site. Retrograde tracing showed that the majority of regenerated axons originated from the raphe nuclei or reticular formation. Another study has shown that the mammalian enzyme arylsulfatase B (ARSB) is also effective in promoting serotonin fiber regeneration by breaking down the inhibitory chains on CSPGs (Yoo et al., 2013). Following a spinal cord compression injury, treatment with either ARSB or ChABC resulted in increased serotonin fiber density at the compression site compared to control treatment with no enzyme. As with the previous studies, this was correlated with a functional recovery, as treated mice scored better on a locomotor activity assessment.

In some cases, peripheral nerve grafts are not necessary for serotonin fiber regeneration following injury, however. Following a spinal cord contusion, grafting Schwann cells that were engineered to secrete ChABC and a neurotrophin was shown to also be sufficient to increase the number of serotonin fibers in the damaged area 12 weeks after injury (Kanno et al., 2014). The increase in serotonin fibers is evident among the grafted cells, in the contused spinal cord, and in the spinal cord caudal to the injury site.

In the neocortex, fixed tissue studies using immunohistochemistry against serotonin, which is expressed through serotonin axons, have shown that following a large dose of amphetamine there is massive serotonin axon degeneration followed by putative regeneration (Molliver et al., 1990). Amphetamine is highly neurotoxic to serotonin fibers and the resulting lesions showed profound serotonin fiber loss in the neocortex 2 weeks after the insult. Over the course of 2 to 8 months, serotonin fiber density increases in the neocortex. The recovery is most rapid in the frontal cortex and most delayed in the parietal cortex, which is indicative of the course that serotonin fibers normally run through this region. While highly suggestive of serotonin regeneration in the neocortex, this evidence remained inconclusive. Because these initial neocortical studies were performed on fixed tissue with serotonin antibodies, the findings could be explained by sprouting axons or refilling of existing axons that had transiently lost their serotonin stores.

Recently the first evidence of long-distance regeneration of serotonin axons in the central nervous system came in the form of *in vivo* two-photon time-lapse microscopy (Jin et al., 2016). Enhanced green fluorescent expressing serotonin axons in a serotonin transporter-EGFP BAC transgenic mouse were imaged over time in three-dimensional space before and for months following an amphetamine lesion. In the imaging area 70% of the axonal length was lost 1 week after amphetamine lesion compared to the baseline. Over 28 weeks, serotonin fiber density in the imaging area increased, returning to around 70% of baseline density. The vast majority of new axonal length that was measured had entered from outside of the imaging plane. While sprouting events from axons that were spared during amphetamine treatment did occur, they were rare, and it was even rarer for these sprouted axons to exit the imaging plane. It is therefore mathematically improbable that sprouting from outside of the imaging area could account for the profound increase in serotonin fiber density and highly suggestive that it is long-distance regeneration from damaged axons that is responsible for the new innervation. The axons that were spared in the amphetamine lesion were stable over time after the lesion. The same was true for regenerated axons; once they entered the imaging area they persisted, sometimes exhibiting further growth in the imaging area. The regenerated axons were morphologically similar to surviving axons, had distributions between fibers similar to fiber distributions in control animals, and exhibited the same degree of tortuosity through the imaging area as surviving axons and axons from control animals. Interestingly, unlike with regeneration in the peripheral nervous system, the regenerated axons did not follow

pathways left by degenerated axons (Scheib and Hoke, 2013). Furthermore, 6 months after amphetamine lesion the regenerated axons were competent to release serotonin as measured by fast-scan voltammetry experiments. These findings, taken together, show that serotonin fibers have the intrinsic ability to regrow in the central nervous system.

However, amphetamine lesion is an unusual insult in that it does not induce a lasting reactive glial response (Wilson and Molliver, 1994). While the diminished regenerative potential of most adult neurons presents the intrinsic barrier to recovery following injury, reactive gliosis is a major extrinsic factor impeding regeneration (Chew et al., 2012). Reactive astrogliosis is initially a beneficial response. Activation of astrocytes serves to limit excitotoxicity through glutamate uptake, protect from oxidative stress, regulate inflammation, and facilitate blood-brain barrier repair (Sofroniew, 2009). With mild injury, or at a distance away from the main insult, this reactive response is transient and astrocytes return to their pre-activated state. However, with severe or prolonged insult this response eventually leads to harmful effects and a persisting mature glial scar. This glial scar serves to impede regeneration both by acting as a physical barrier as well as through expression of molecules that strongly inhibit regeneration (Ohtake and Li, 2015). The mature glial scar is also comprised of inflammatory cells, such as microglia and invading macrophages, which can themselves become dysregulated and further inhibit repair (Loane and Kumar, 2015).

Regenerating serotonin fibers appear to be able to overcome these extrinsic inhibitory environments as well. In a spinal cord transection injury model there is evidence for serotonin fibers traversing across reactive astroglial bridges that span the injury site (Lee et al., 2010). In cortex, serotonin fibers were observed to grow further into a glial scar secondary to a thermal lesion than were non-serotonergic fibers (Hawthorne et al., 2011). Again, however, the most conclusive evidence came from two-photon *in vivo* time-lapse imaging of enhanced green fluorescent fiber expressing serotonin fibers. Following a penetrating stab injury through all cortical layers, which does result in a glial scarring, serotonin fibers were observed traversing the injury site (Jin et al., 2016). The penetrating stab injury completely severed all of the serotonin axons within the stab rift, with the cut ends of the fibers regressing no further than a few microns from the rift. Beginning at one week after injury, some new growth was observed from the cut end of the axons. By eighteen weeks post-stab, axonal length in the stab rift had returned to 80% of the baseline axonal length. The newly grown axons in the stab rift were also able to form new branchpoints within the stab rift.

However, neither the amphetamine lesion nor the penetrating stab injury are the most clinically common injuries, so whether this regenerative capacity remains in typical traumatic brain injury remains an open question.

Traumatic brain injury

Traumatic brain injury (TBI) is a physical injury that results in the disruption of normal brain function. In the United States there are approximately 2.5 million emergency department visits involving TBI annually, a number which likely underestimates the true incidence (Centers for Disease Control and Prevention, 2015). TBI affects all age groups, but at specific risk are children (age 0-4), adolescents (age 15-19) and the elderly (age >75). The cause of injury across these age groups also differs. The children and elderly are at highest risk for TBI secondary to a fall, while adolescents are most at risk of TBI as a result of motor vehicle accidents (Faul and Coronado, 2015). Severity of TBI varies across the population as well. While children are twice as likely to be brought to an emergency department and diagnosed with a TBI as the elderly, the elderly are more likely to require hospital admission (Faul and Coronado, 2015). Across all age groups, the highest mortality rate is for TBI in motor vehicle accidents. Between 2007 and 2010 there was a large increase in emergency hospital visits for TBI while mortality from them continued to decrease. This is most likely due to the recent increased awareness of TBI, especially in the context of sports-related injuries in adolescents, while technology improvements continue to decrease mortality in motor vehicle accidents (Centers for Disease Control and Prevention, 2015). It is therefore important to note that TBI is not a discrete injury type, but rather a range of injury types that have diverse outcomes depending on the patient population and mechanism of injury. Studies on experimental animal models should therefore reflect this heterogeneity of insults.

Traumatic brain injury can be caused by a blow against or jolt of head, a penetrating injury to the head, or exposure to blast. TBI secondary to a blow or jolt of the head is most common. The severity of blows or jolts is generally based on the cause of impact. Impacts from sport activities tend to be milder, falls have moderate intensity impacts, and motor vehicle accidents have the highest likelihood of resulting in severe blows or jolts. It should be noted that these are only general trends; for instance, a fall from a large height has the potential to result in a higher energy impact than a motor vehicle accident at very low speeds. Likewise, not every blow or jolt, no matter how severe, results in TBI (Corrigan et al., 2010). Together, these injuries tend to damage tissues through biomechanical forces generated by rapid acceleration, deceleration, compression against the intact skull, and changes in intracranial pressure. Penetrating injuries cause damage through both impact and directl damage to brain tissue and brain vasculature. Blast injuries, which are most common among military personnel, are least understood, but evidence suggests that damage to the brain may be due to systemic effects of blasts such as disruption of lung tissue and subsequent hypoxia (Long et al., 2009).

While the initial insult or insults resulting in TBI can be thought of as a discrete event, TBI itself is a chronic disease process (Masel and DeWitt, 2010). Following rehabilitation after injury, patients with TBI are at greater risk of death than controls, with an estimated seven year reduction in life expectancy (Harrison-Felix et al., 2004). Traumatic brain injury

patients are also at an increased risk for a wide range of morbidities, including neurological disorders (such as epilepsy), neurodegenerative diseases (such as Alzheimer's dementia), and psychiatric disease (such as major depression) (Masel and DeWitt, 2010).

Major depression is the most commonly reported neurobehavioral sequela of TBI (Riggio and Wong, 2009). While the actual prevalence of major depression following TBI is debated in the literature (reported values range from 27 to 61%) it is accepted that the rate is higher than the 17% seen in general population (Jorge et al., 2004). The causal link between TBI and depression remains unclear. One of the best predictors for the development of depression after TBI is a history of previous psychiatric illness, which suggests that TBI may lead to depression by exacerbating previous pathologies (Riggio and Wong, 2009). In terms of clinical findings, lesions to the left dorsolateral frontal cortex and left basal ganglia are most strongly correlated with the development of depression (Fedoroff et al., 1992). Traumatic brain injury may, therefore, be a result of disruption of executive function via the frontal-striatal-thalamic circuit. Another possibility is that disruption of normal monoaminergic modulation of the prefrontal cortex is responsible for the cognitive defects in post-TBI depressed patients. The monoamine hypothesis of depression states that an imbalance in monoamine, especially serotoninergic, neurotransmission is the biological basis of the disease. While this hypothesis is unlikely to explain all facets of depression, there is amble evidence to support its contributory role

in the pathophysiology of depression, along with involvement of the neuroendocrine stress axis, neuroinflammation, and neurotrophic signaling (Kohler et al., 2016). Indeed, the first line of treatments for depression following TBI are the selective serotonin reuptake inhibitors, which target the serotonergic transporter to increase serotonin concentration in the central nervous system (Silver et al., 2009).

Given the unique capacity for serotonin fibers to regenerate in certain conditions and the role of the serotonergic system in neurobehavioral sequelae of TBI, the question of whether serotonin fibers undergo damage and are able to regenerate following TBI is of great interest. The experiments in this dissertation begin to answer these questions.

Chapter 2: General Methods

All animal procedures were performed in compliance with National Institutes of Health guidelines and all protocols were approved by the Johns Hopkins School of Medicine Institutional Animal Care and Use Committee.

Controlled cortical impact injury (CCI) protocol

10 week old female C57BL/6 mice (Charles River) were first induced with 3% isoflurane anesthesia in a closed plastic container and the skull was then shaved in preparation for surgery. Mice were then placed in the stereotaxic device (Stoelting) with 1.5% isoflurane delivered via a nose cone. The skin above the skull was cleaned with alcohol and iodine and a midline incision was made to expose the skull. The skin was retracted medially and held in place with a modified Colibri retractor (Fine Science Tools). Fascia was removed from the skull and a round craniotomy was made with a 2.7 mm trephine drill bit (Fine Science Tools) using an electric drill. The craniotomy location was over the left hemisphere of the brain; the medial aspect of the craniotomy was against the sagittal suture and the antero-posterior aspect of the craniotomy was centered on the coronal suture. The skull over the craniotomy was carefully removed using a scalpel and tweezers, and the dura was inspected to ensure that it remained intact.

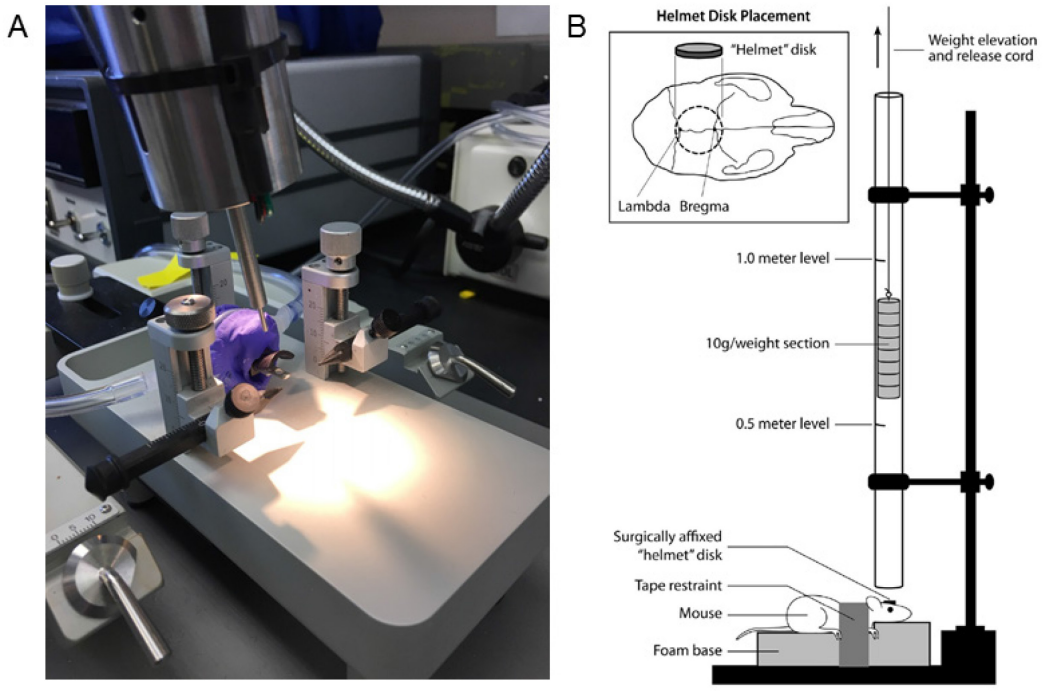

Figure 2. Impactors for the induction of traumatic brain injury. A) The Leica electromagnetic impactor used for controlled cortical impact (CCI) surgeries is pictured mounted to the stereotaxic device. B) A schematic of the setup used for repetitive mild traumatic brain injury surgeries. Panel B is reproduced from Xu et al., 2016.

The electromagnetic impactor with a 1.5 mm tip (Leica) was then mounted to the stereotaxic device and centered over the craniotomy site at a 10 degree angle (Figure 2A). This angle results in the impactor being perpendicular to the brain surface under the craniotomy. The impactor was extended and the tip lowered until it made contact with the dura, as measured by the completion of an electrical circuit between the impactor and a wire clipped to the mouse tail. The impactor was then retracted and the impact depth was set to 0.75 mm past the measured surface of the dura. The electromagnetic impactor

was then activated resulting in an impact with a final velocity of 4 m/s and a dwell time of 100 ms. These parameters were chosen from a wide range of empirically tested values (see Table 1) to provide an injury that was consistent across animals, resulted in visible damage to neocortical layers 1, 2/3 and 4, and largely spared neocortical tissue anterior and posterior to the injury site to allow for analysis of fixed tissue in those areas.

Injury Parameters	Values Used
Craniotomy Diameter (mm)	2.7, 3.6, 5.0
Impactor Diameter (mm)	1.0, 1.5, 3.0
Impact Depth (mm)	0.33, 0.50, 0.75, 0.80, 1.00
Impact Velocity (m/s)	0.5, 1.0, 4.0
Impact Angle (degrees)	0, 10

Table 1. Parameters of controlled cortical impact that were varied to adjust the severity of injury. Craniotomy diameter and impactor diameter value increments were based on availability of trephine drill bits and metal impactor tips. Impact depth and angle were set via the stereotaxic device, while impact velocity was adjusted on the electromagnetic impactor controller. Dwell time was kept constant at 100 ms throughout testing different parameter permutations.

After impact the retractor was removed and the skin was closed above the craniotomy using 9 mm wound clips (Fine Science Tools). Mice were given subcutaneous injections of Baytril (2.5 mg/kg) to prevent infection and Buprenex (0.01 mg/kg) for pain

management. Mice were removed from the stereotaxic device and put in a recovery cage on their backs. Righting time, defined as the amount of seconds it took for the mice to flip and place all four paws on the bedding, was measured to assess the immediate injury severity (control: range 9-144, median 46; open skull: range 39-650, median 214; CCI: range 36-597, median 301). Mice were then returned to group housing for the duration of the post-surgery time point. Open skull control mice received the same treatment, but the impactor was not fired. Control mice received the same treatment, but did not receive a craniotomy, and the impactor was not fired. Animals were sacrificed for tissue processing either 1 week, 1 month, or 3 months after surgery.

Repetitive mild traumatic brain injury protocol

Female C57BL/6 mice (Charles River) 8 weeks of age were anesthetized with an isoflurane, oxygen, nitrous oxide mixture (1:33:66, respectively). The skin above the skull was cut along the sagittal suture and the remaining fascia was removed. A 3.2 mm diameter, 1 mm thick steel disc was glued onto the skull with cyanoacrylate glue. The disc was centered on the sagittal suture and extended to cover both the coronal and lambdoid sutures. The mice were removed from anesthesia and quickly placed on a foam mat (Foam to Size, Inc.) with the metal disc centered underneath a plexiglass tube (Figure 2B). Tape was used to restrain the animal. Stacked metal weights (40 g total, 10 g per section) were affixed to a string and elevated in the plexiglass tube to a height of 1 m above the metal disc. The string was then released and the weight assembly was allowed to impact the

metal disc. The animal was immediately moved after the initial impact to prevent a rebound impact. The mice were removed from the foam bed and breathing was monitored. If spontaneous breaths were not immediately observed, a few forced mechanical breaths were provided. After self-righting, the mouse was anesthetized again and the metal disc was removed. The skull was checked to confirm absence of fracture and the skin was closed with would clips (Fine Science Tools). The mice were then returned to group housing for the duration of the study.

For mice in the 1x impact group, this procedure was performed once on day 0. For mice in the 4x impact group, the above procedure was repeated on day 0, day 1, day 3, and day 7. For mice in the 8x impact group, the above procedure was repeated on the same days as the 4x impact group, but each animal received 2 impacts, approximately 1 hour apart. The metal disc was not removed in between impacts delivered on the same day. Sham animals underwent the same treatment but did not receive any impacts. The final day of impacts was treated post-surgical day 0, and all animals were sacrificed 7 days post-surgery (i.e., 14 days after the initial impact).

Tissue processing

Mice were anesthetized with a mixture of ketamine (100 mg/kg) and xylazine (10 mg/kg) and perfused intracardially with ice-cold 0.01 M phosphate-buffered saline (PBS) followed by ice-cold 4% paraformaldehyde (PFA) in PBS. After perfusion, the brain was

removed and placed in 4% PFA in PBS at least overnight at 4 °C. Two days prior to slicing, brains were cyroprotected in 15% sucrose in PBS overnight at 4 °C followed by 30% sucrose in PBS overnight at 4 °C. The left hemisphere of samples was then sectioned into 40 μm thick slices on a freezing sliding microtome. The slices were stored in PBS at 4 °C.

Immunohistochemistry and image acquisition

For the CCI experiments, tissue from all three treatment groups at each time point was processed together. Sections were washed with 0.3% Triton X-100 in PBS and blocked in 5% normal goat serum and 0.3% Triton X-100 in PBS for 2 hours at room temperature. The sections were then incubated with primary antibody in the blocking buffer overnight at 4 °C. The primary antibodies used were guinea pig anti-SERT (Frontier Institute #HTT-GP-Af1400), mouse anti-NeuN (Millipore #ABN60), chicken anti-GFP (Aves Labs #GFP-1010), rabbit anti-GFAP (Millipore #AB5804), and rabbit anti-Iba1 (Wako #019-19741). For SERT/NeuN, GFAP/NeuN, and Iba1/NeuN double staining, the primary antibody dilutions were all 1:1000. For SERT/YFP/NeuN triple staining the dilutions were 1:1000, 1:5000, and 1:500, respectively. Slices were washed in PBS and incubated with secondary antibody diluted in blocking buffer at room temperature for 2 hours. The secondary antibodies used were FITC-labeled goat anti-guinea pig (1:1000, Invitrogen #A18776), Alexa Fluor 594-labeled goat anti-mouse (1:500, Jackson ImmunoResearch Laboratories #115-586-062), Alexa Fluor 488-labeled goat anti-rabbit (1:500 Jackson ImmunoResearch Laboratories #111-546-003), Cy3-labeled goat anti-guinea pig (1:800, Jackson

ImmunoResearch Laboratories #106-165-003), Cy5-labeled goat anti-mouse (1:200, Jackson ImmunoResearch Laboratories #115-175-146) and FITC-labeled goat anti-chicken (1:1000, Invitrogen #A16055). The Alexa Fluor labeled secondary antibodies were reconstituted with water and diluted 1:1 with glycerol; all other secondary antibodies were reconstituted with water only. The sections were washed again and mounted on slides for imaging. A single photon laser scanning confocal microscope was used to acquire all images (Zeiss LSM 510). Imaging of tissue that was processed together was performed with the same settings and laser power for each sample. Experimenters were blinded to the treatment groups, which were interleaved throughout the imaging process.

Image analysis

Raw acquired images were exported from Zeiss LSM software in an uncompressed tagged image file format and stored for subsequent analysis using custom code written using the Anaconda Python distribution (Continuum Analytics). Imaging z-stacks were maximally projected and the projection was used to set a threshold for detection of pixels positive for SERT or Iba1 immunohistochemistry. The threshold was calculated using an iterative algorithm for feature extraction (Ridler and Calvard, 1978). The threshold is set to 0 to begin and is incrementally increased until the following condition is true (a background pixel is any pixel at or below threshold; an object pixel is any pixel above the current threshold):

$$threshold > \frac{average\ background\ pixel\ value + average\ object\ pixel\ value}{2}$$

After the threshold has been calculated it is applied to an image such that every background pixel is set to 0 (black) and every object pixel is set to 255 (the highest value for an 8-bit image). This serves as an unbiased systematic contrast enhancement technique that allows for the subsequent calculation of pixels positive for a given signal (Figure 3).

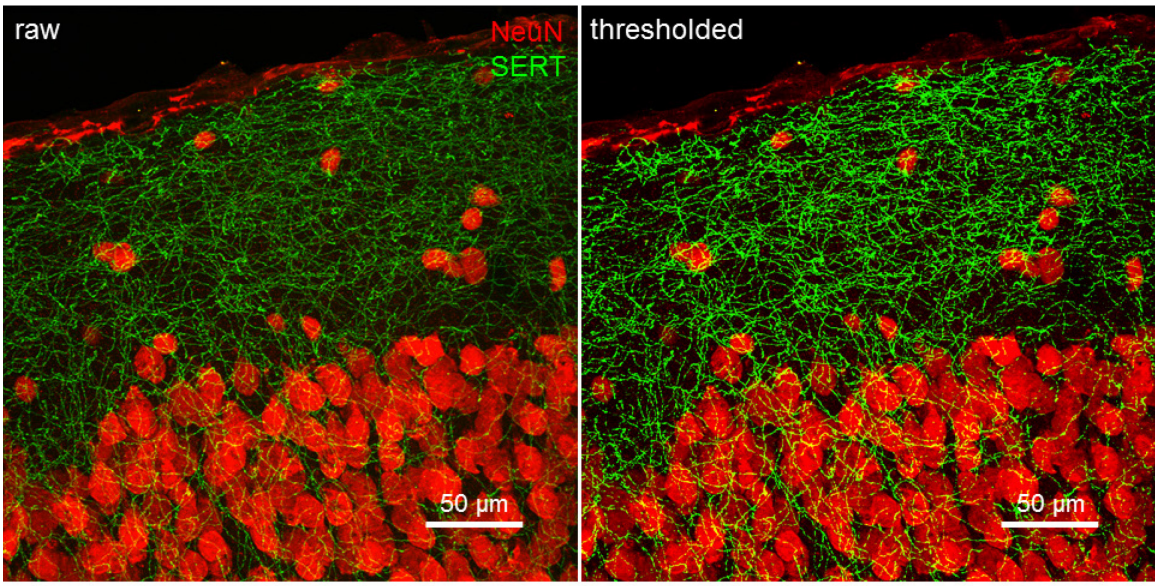

Figure 3. Example of thresholding algorithm output applied to an image of double-label immunohistochemistry. The left image shows a maximally projected z-stack before thresholding. The right side shows the same image after applying the threshold to the green channel. Each z-stack contained 41 images, 1 µm apart.

For the quantification of serotonin fiber density, the threshold was applied to each slice of the z-stack before the maximal projection was created. The number of pixels above threshold in each individual slice was summed together and expressed as the percent of

pixels above threshold, where the total number of pixels was the two-dimensional maximally projected area. Exemplar images were generated using the same method. This approach was used to account for the fact that in a maximally projected image any area where serotonin fibers run in the z-direction would result in an underestimate of fiber density in the two-dimensional projection. For quantification of microglial density, a 10 μm maximal projection was generated from the top of the imaging stack, the threshold was applied, and quantification was performed on the projected image.

For quantification of reactive astrocytes, a manual counting method was employed on 10 μm maximally projected images, taken from the top of the 40 μm imaging stack. All GFAP-positive cells that matched the distinct morphology of reactive astrocytes within the layer of interest were counted. In layer 1, GFAP-positive cells that were part of the pia mater were excluded. To confirm that manual cell counting was an accurate measure, counts in layer 1 were compared to the percent pixels above threshold measure and were found to match closely (not shown).

Statistics

Statistical significance was determined using a linear regression model followed by targeted t-tests adjusted for multiple comparisons. Data was divided based on imaging regions and the dependent variable. For each data set, an ordinary least squares regression model was run, fitting the data to take into account the effect of treatment group, time,

and the interaction between treatment group and time. If the linear model suggested an effect of the regressors for the group, one-tailed heteroscedastic t-tests were performed within a timepoint across groups and across timepoints within a group. These results of the t-tests were adjusted for multiple comparisons using the Bonferroni correction. Data is presented as means ± the standard error of the mean. Significance throughout the text is denoted as follows: * indicates $p < 0.05$, ** indicates $p < 0.01$, and *** indicates $p < 0.001$.

Chapter 3: Controlled Cortical Impact and 5-HT Fiber Innervation

There is evidence that serotonin fibers can regenerate in the central nervous system, both in spinal cord (Lee et al., 2013) and neocortex (Jin et al., 2016). However, the neocortical injury models used in these experiments reflect unique insults. The amphetamine lesion does not create a glial scar (Wilson and Molliver, 1994), while the penetrating injury is less common clinically and leaves a relatively narrow rift to be crossed. Therefore, whether serotonin fibers are able to regrow following clinically relevant traumatic brain injury remains unknown. To address this question we analyzed serotonin fiber density following controlled cortical impact injury in mice.

Serotonin fibers regrow following TBI

Young adult mice (10 weeks old) were exposed to one of three treatment groups. The CCI group which received a craniotomy and an impact directly to the dura, the open skull group which received a craniotomy but no impact, and a control group that received neither a craniotomy nor impact. All groups received anesthesia, an incision, wound clips, and post-operative drugs. Mice were sacrificed at 1 week, 1 month, and 3 months post-surgery.

Double-label immunohistochemistry was performed on sagittal sections of brain corresponding to the middle of the craniotomy (lateral +1.32 mm) to visualize the extent

of serotonin fiber damage and recovery following injury. Serotonin fibers were labeled with an antibody against the serotonin transporter SERT, which is expressed throughout the axon of serotonergic cells. In order to be able to identify neocortical layers, neuronal cell bodies were visualized with an antibody against NeuN, which is expressed in most mature neuronal nuclei.

Low magnification images were taken first to assess the extent of the injuries. One week post-surgery there was always an obvious physical deformation in the upper layers of the motor cortex in the CCI group (Figure 4). This damage involved layers 1, 2/3, and 4. In the open skull condition there was occasional damage confined to layers 1 (n = 15 out of 26) and 2/3 (n = 10 out of 26) underneath the craniotomy site. There was never damage to the neocortex in the control group.

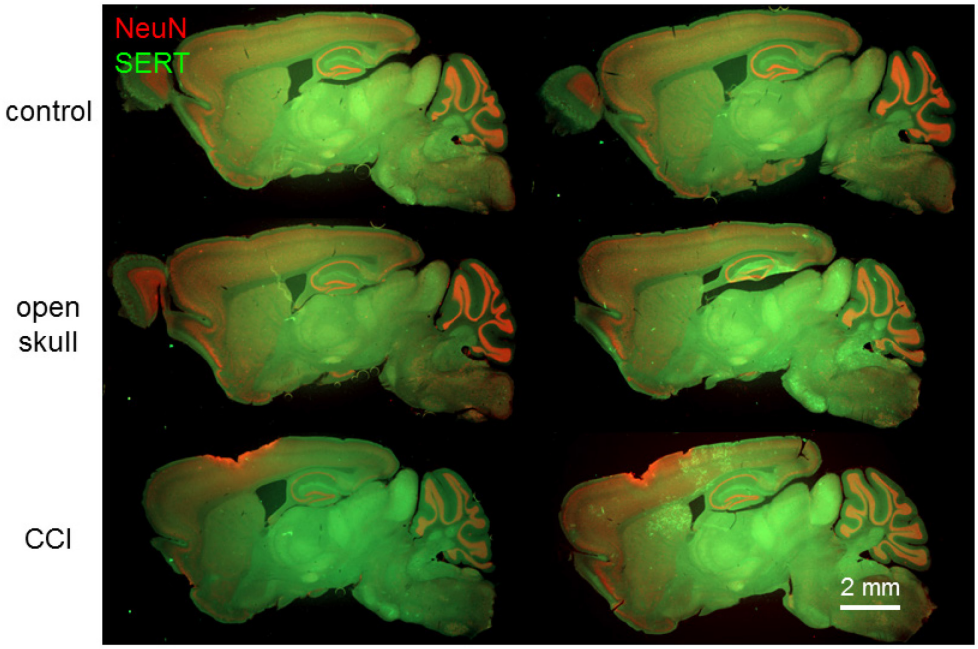

Figure 4. Low magnification exemplar images of sagittal sections reveal the extent of injury evoked by controlled cortical impact in 2 exemplar mice per group. One week post-surgery the damage inflicted by controlled cortical impact is apparent (bottom row). The open skull group (middle row) and control groups (top row) have entirely intact neocortex. Occasionally damage secondary to the open craniotomy can be observed in the open skull condition (middle row, right side, above the lateral ventricle).

Next, single-photon 40x confocal stacks were acquired to visualize serotonin fibers at several anatomical locations. Since serotonin fibers run in an anterior to posterior gradient in the neocortex (Figure 1), we wanted to observe damage and recovery both anterior (proximal) to the injury, where we predicted there would be relatively little damage, and posterior (distal) to the injury, where we predicted there would be significant fiber loss

due to axonal damage within the injury zone. The anterior and posterior areas were chosen to border either edge of the craniotomy location (anterior aspect: Bregma +1.34 mm; posterior aspect: Bregma -1.34 mm). By choosing constant imaging areas we minimized between-animal variation in serotonin fiber due to the antero-posterior density gradient. We were also interested in whether any differences in damage and recovery exist among different cortical layers, for instance as a result of different serotonin fiber innervation patterns of the dorsal and median raphe projections (Vitalis et al., 2013). To this end, we imaged regions including layer 1, layer 2/3, and layer 4, both anterior and posterior to injury. Sections from open skull and control animals were imaged in corresponding regions.

The SERT signal from the raw confocal stacks was contrast enhanced using an iterative thresholding algorithm and was maximally projected along with the raw NeuN signal to allow visualization and quantification of serotonin fiber density. Quantification was performed by summing pixels above threshold and expressing this is a percent of the total number of pixels in the region of interest (i.e. layer 1, 2/3, or 4 as drawn by hand, guided by the NeuN images). The percent pixels above threshold measure was then normalized to the control condition within each time point to allow comparisons between time points (which did not undergo tissue processing, immunohistochemistry, and imaging together).

Anterior to the injury site in layer 1 there was a small decrease in serotonin fiber density in both the open skull (78.5 ± 8.9%, n = 9) and CCI conditions (78.6 ± 13.3%, n = 7) when measured one week post-surgery compared to control (100.0 ± 5.4%, n = 8) (Figure 5). These decreases were not statistically significant (Figure 7; t-test $p > 0.0125$).

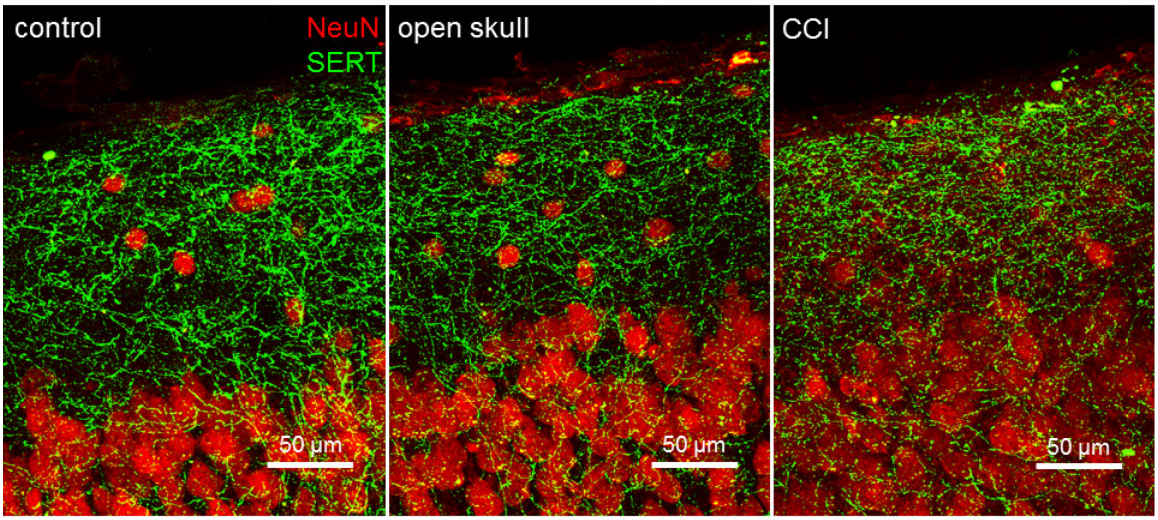

Figure 5. Exemplar images show 5-HT fiber innervation in neocortical layer 1 anterior to the CCI injury site, one week after surgery. Maximally projected 40x confocal z-stacks with thresholded SERT signal show a small decrease in serotonin fiber innervation in the open skull (middle) and CCI groups (right) compared to the control group (left). Damage due to impact can be appreciated in the CCI group by the deterioration of the NeuN signal.

Layers 2/3 and 4 anterior to the injury site show a similar pattern of serotonin fiber loss as layer 1 when measured one week post-surgery (Figure 6). Neither the open skull group

(layer 2/3: 87.5 ± 4.5%, n = 9; layer 4: 87.4 ± 4.7%, n = 9), nor the CCI group (layer 2/3: 85.5 ± 8.2%, n = 7; layer 4: 96.0 ± 6.8%, n = 7) showed significant serotonin fiber loss compared to the control group (layer 2/3: 100.0 ± 2.6%, layer 4: 100.0 ± 5.5%, n = 8).

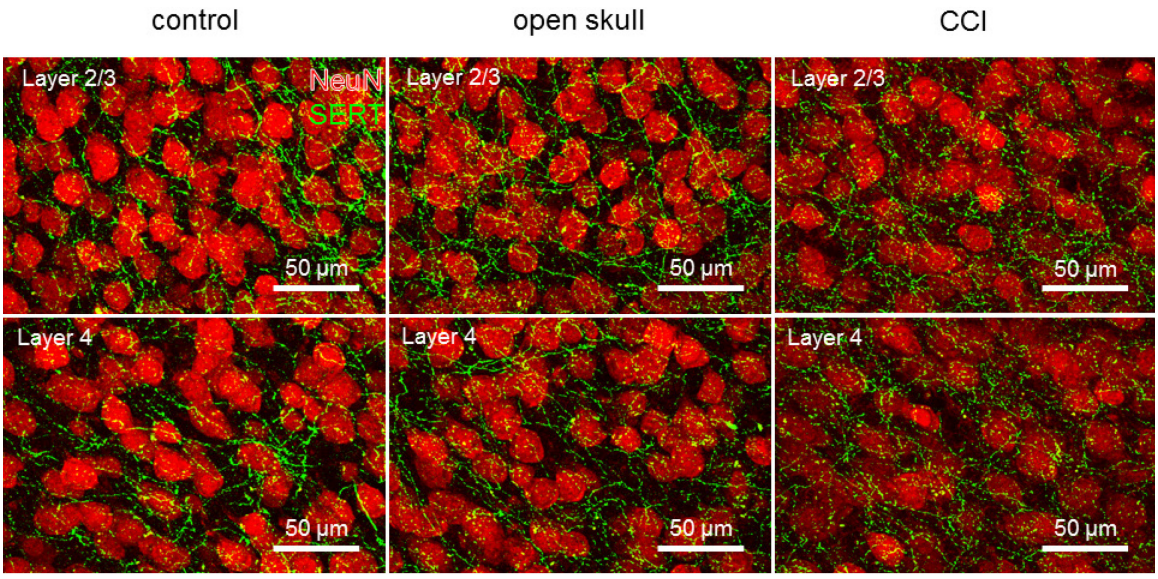

Figure 6. Exemplar images show 5-HT fiber innervation in neocortical layers 2/3 and 4 anterior to the CCI injury site, one week after surgery. Maximally projected 40x confocal z-stacks with thresholded SERT signal show little decrease in serotonin fiber density of layer 2/3 (top row) and layer 4 (bottom row) in the open skull (middle) and CCI groups (right) compared to the control group (left).

Serotonin fiber density was also quantified in these areas one month and three months post-surgery (Figure 7). One month post-surgery serotonin fiber density was similar in layer 1 among all treatment groups. Serotonin fiber density was also similar between the

groups in layer 2/3 and layer 4. There was no appreciable increase in serotonin fiber density from one month to three months post-surgery in layer 1, layer 2/3, or layer 4.

In summary, there were no differences in serotonin fiber density anterior to the injury site one week post-surgery. One month and three months after injury, serotonin fiber density remained indistinguishable between the treatment and control groups in all layers.

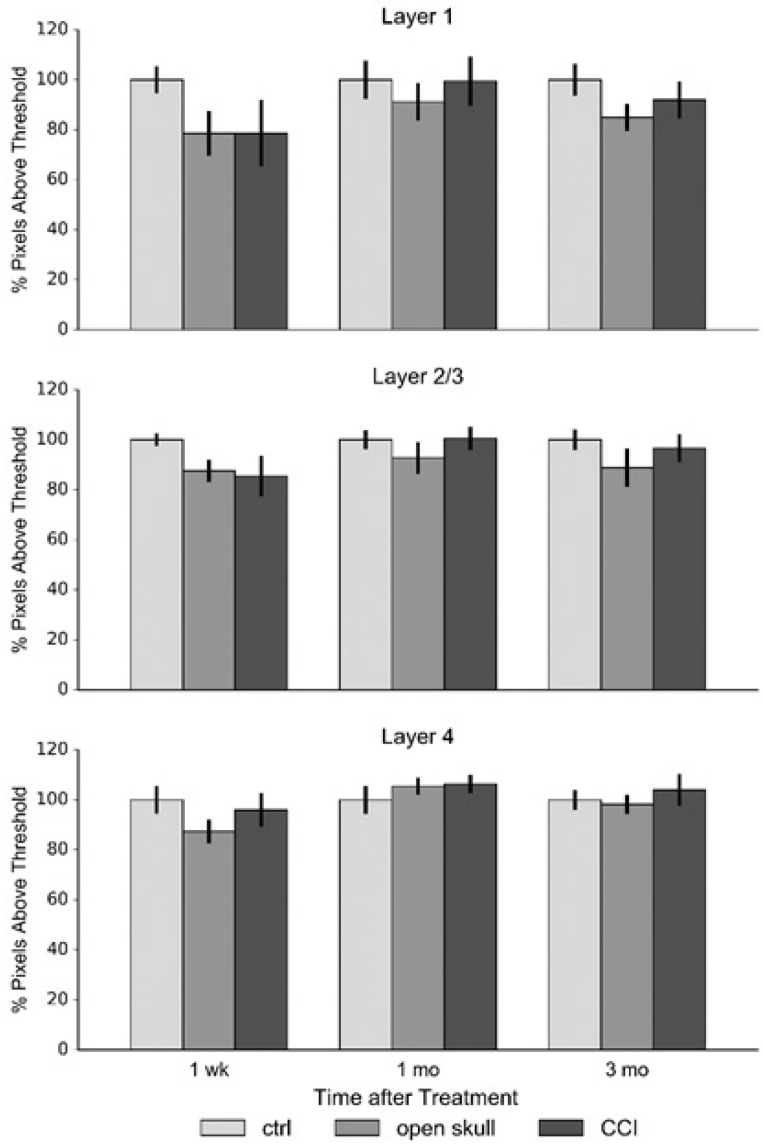

Figure 7. Quantification of 5-HT fiber innervation anterior to the CCI injury site. Percent of SERT pixels above threshold was calculated to quantify serotonin fiber density. The data were normalized to control levels for each layer and time point. There was no significant fiber loss anterior to the injury site following treatment one week post-surgery and no change was noted one month and three months post-surgery.

In contrast to the region anterior to the injury site, there was a significant decrease in serotonin fiber density in layer 1 posterior to the injury site, when measured one week post-surgery (Figure 8). This decrease was present in both the open skull group (54.8 ± 6.8%, n = 9, $p < 0.001$) and CCI group (45.7 ± 9.6%, n = 7, $p < 0.01$) compared to the control group (100.0 ± 6.4%, n = 8).

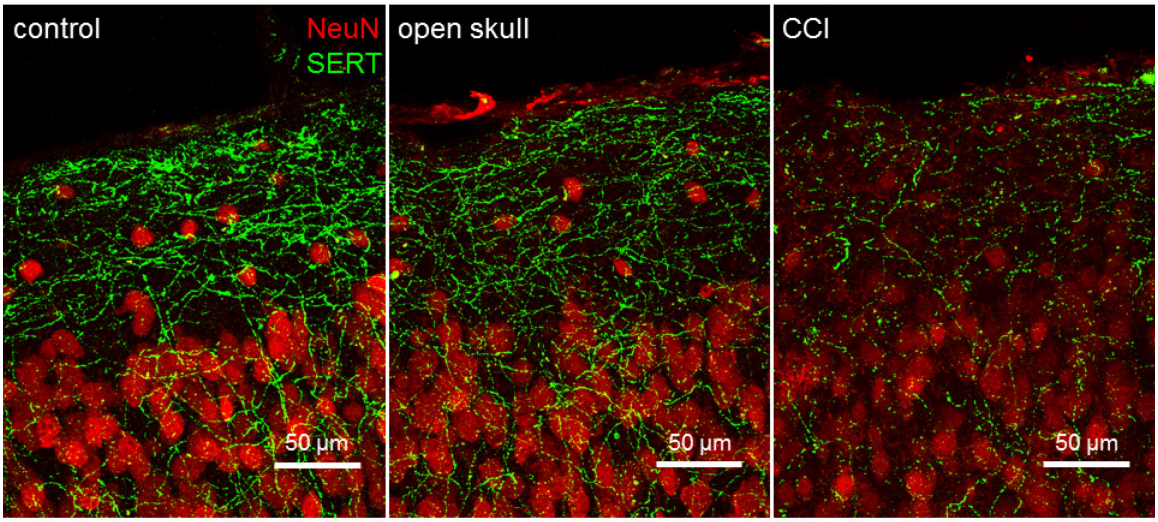

Figure 8. Exemplar images show 5-HT fiber innervation in neocortical layer 1 posterior to the CCI injury site, one week after surgery. Maximally projected 40x confocal z-stacks with thresholded SERT signal show a significant serotonin fiber density decrease in both the open skull (middle) and CCI groups (right) compared to the control group (left). Serotonin fiber density in the control group posterior to the injury site is lower than anterior to the injury site due to the normal antero-posterior distribution of serotonin fibers in neocortex.

We also measured serotonin fiber density in deeper neocortical layers in this area (Figure 9). In layer 2/3 posterior to the injury site there is a significant decrease in serotonin fiber density in the open skull group (79.7 ± 4.4%, n = 9, $p < 0.016$) compared to the control group (100.0 ± 5.9%, n = 8), but the decrease in the CCI group (79.9 ± 7.2%, n = 7) is not statistically significant after correction for multiple comparisons (t-test, $p > 0.016$). In layer 4 there were no significant differences ($p > 0.016$) one week post-surgery compared to the control group (100.0 ± 3.6%, n = 8) for either the open skull (89.1 ± 4.3%, n = 9) or CCI (80.8 ± 7.3%, n = 7) groups despite a trend toward decreasing innervation.

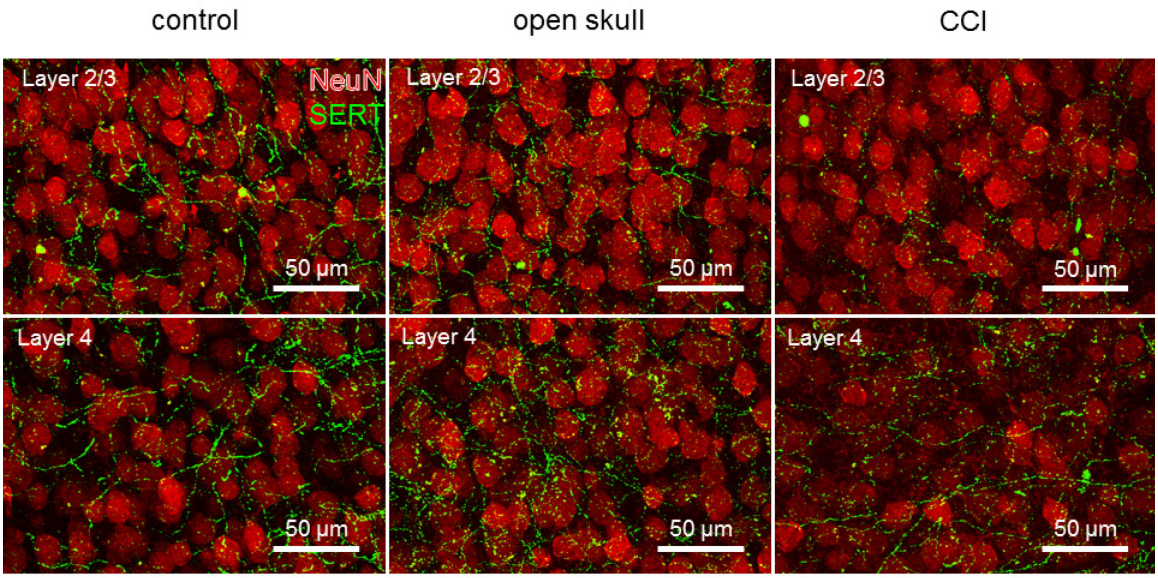

Figure 9. Exemplar images show 5-HT fiber innervation in neocortical layers 2/3 and 4 posterior to the CCI injury site, one week after surgery. Maximally projected 40x confocal z-stacks with thresholded SERT signal show a decrease in serotonin fiber density

of layer 2/3 (top row), but no significant decreases in layer 4 (bottom row) in the open skull (middle) and CCI groups (right) compared to the control group (left).

These results show that serotonin fibers are damaged following traumatic brain injury, either from an open craniotomy alone or CCI, and that serotonin fiber density is decreased posterior but not anterior to the injury site, consistent with their anterior-to-posterior / proximal-to-distal direction. Given this finding, that serotonin axon density is decreased in layer 1, posterior to injury, 1 week post-surgery, we sought to determine whether serotonin fibers are capable of regrowth following traumatic brain injury.

In layer 1, posterior to the injury site, there was an increase in serotonin density for the open skull condition at one month (77.4 ± 8.3%, n = 8) and three months (68.7 ± 2.2%, n = 9), but these increases were not statistically different from the density observed at one week post-surgery. However, there was significant recovery of serotonin fiber denisty observed in the CCI group (Figure 10). Density at one month (81.3 ± 8.7%, n = 6, $p < 0.01$) and three months (72.0 ± 6.1%, n = 6, $p < 0.05$) post-surgery were both significantly greater than the density observed one week post-surgery. The density for the control group did not change over time (one month: 100.0 ± 7.8%, n = 8; three months: 100.0 ± 5.6%, n = 8).

In layer 2/3 posterior to the injury site there was no significant difference (t-test, $p > 0.016$) in innervation between groups at when measured one month post-surgery(control: 100.0

± 4.8%, n = 8; open skull: 85.0 ± 5.2%, n = 8; CCI: 94.5 ± 6.9%, n = 6). However, at three months post-surgery density for both the open skull (74.1 ± 6.5%, n = 9, $p < 0.01$) and CCI (80.7 ± 6.9%, n = 8, $p < 0.05$) groups were significantly lower than the control (100.0 ± 5.3%, n = 8) group. Density in layer 4 was not statistically different at one week post-surgery and this remained constant at one month (control: 100.0 ± 5.9%, n = 8; open skull: 93.2 ± 7.1%, n = 8; CCI: 91.0 ± 3.7%, n = 6) and three months (control: 100.0 ± 4.2%, n = 8; open skull: 83.7 ± 4.2%, n = 9; CCI: 90.8 ± 6.0%, n = 8) post-surgery.

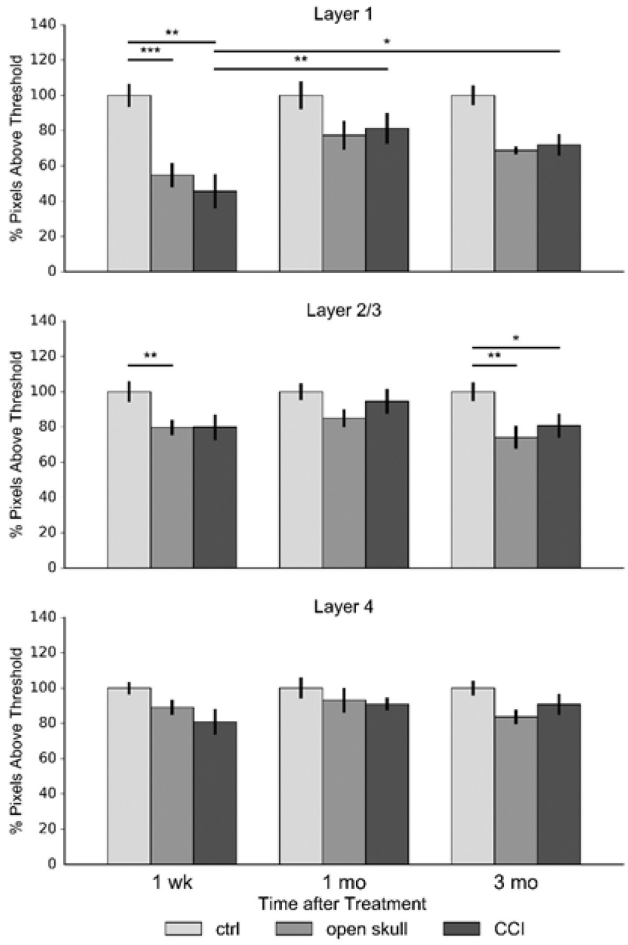

Figure 10. Quantification of 5-HT fiber innervation posterior to the CCI injury site. Percent of SERT pixels above threshold were calculated to quantify serotonin fiber innervation. The data was normalized to control levels for each layer and time point. There was significant serotonin fiber loss following treatment one week post-surgery. Significant regrowth was evident in the CCI group at one months and three months compared to one week. * indicates $p < 0.05$, ** indicates $p < 0.01$, *** indicates $p < 0.001$.

Taken together these results support the conclusion that traumatic brain injury leads to serotonin fiber damage in superficial layers posterior to the injury site and that, in layer

1, serotonin fibers are able to regrow one month and three months following a clinically relevant injury model (Figure 11).

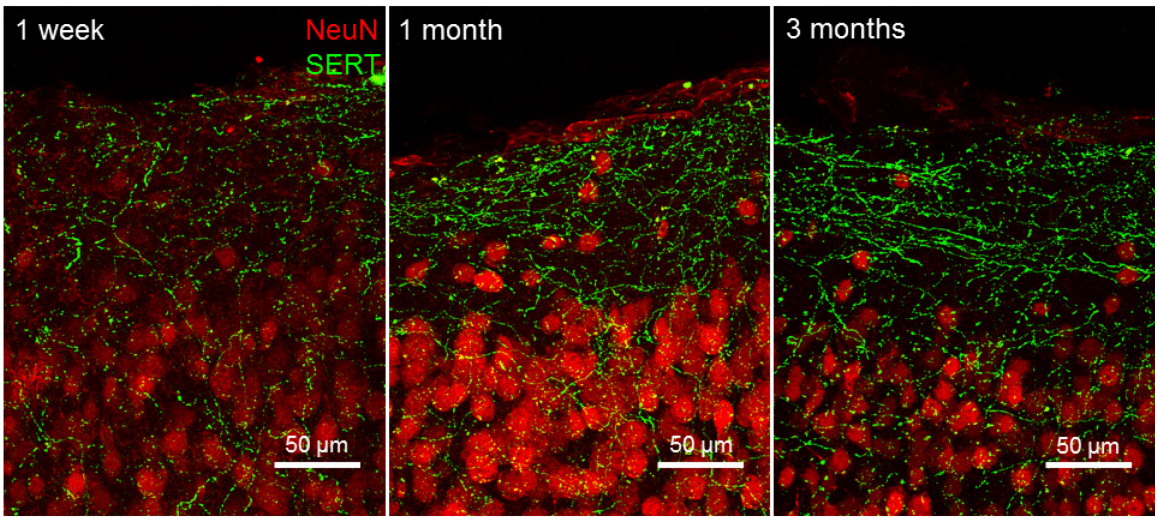

Figure 11. Exemplar images show recovery of 5-HT fiber innervation in neocortical layer 1, posterior to the CCI injury site. Following profound serotonin fiber loss (left; 45.7 ± 9.6%) one week post-surgery, serotonin fibers are able to re-innervate the damaged neocortex one month (middle; 81.3 ± 8.7%) post-surgery with fibers. This recovery persists at least three months post-surgery (right; 72.0 ± 6.1%).

One potential confound to this interpretation is that controlled cortical impact or open skull injury might result in a decrease in expression of SERT posterior to the injury site, rather than a true loss of fibers. Under this scenario, the decrease in serotonin density would be an artifact of this expression change and the perceived regrowth could be explained by the return of SERT expression in undamaged fibers. To address this issue,

we repeated the controlled cortical impact protocol on serotonin transporter-Cre mice that received injections of the virus AAV5-EF1a-DIO-hChR2(H134R)-EYFP-WPRE-pA (Tsai, 2009) in the dorsal raphe. This yields mice in which infected dorsal raphe serotonin neurons, and their neocortical axon projections, have surface membrane YFP that is constitutively expressed, under the control of the viral EF1a promoter rather than the native SERT promoter. We were then able to perform triple label immunohistochemistry to identify EYFP positive serotonergic axons, SERT positive serotonergic axons, and NeuN to identify neocortical layers. To measure fiber loss following injury, both the SERT and EYFP signals were processed using the iterative thresholding algorithm described above (Figure 12). Of the SERT positive axons, 26.9% were EYFP positive in the control. We found that following CCI the SERT signal was decreased to 45.5% of the control level and the EYFP signal was reduced to 43.2% of the control level. This strongly argues against the possibility that changes in SERT expression are being misinterpreted as serotonin fiber loss and regrowth. This finding is consistent with results from an amphetamine lesion experiment utilizing the same viral expression approach, which also showed consistency between SERT and YFP signal loss (Jin et al., 2016).

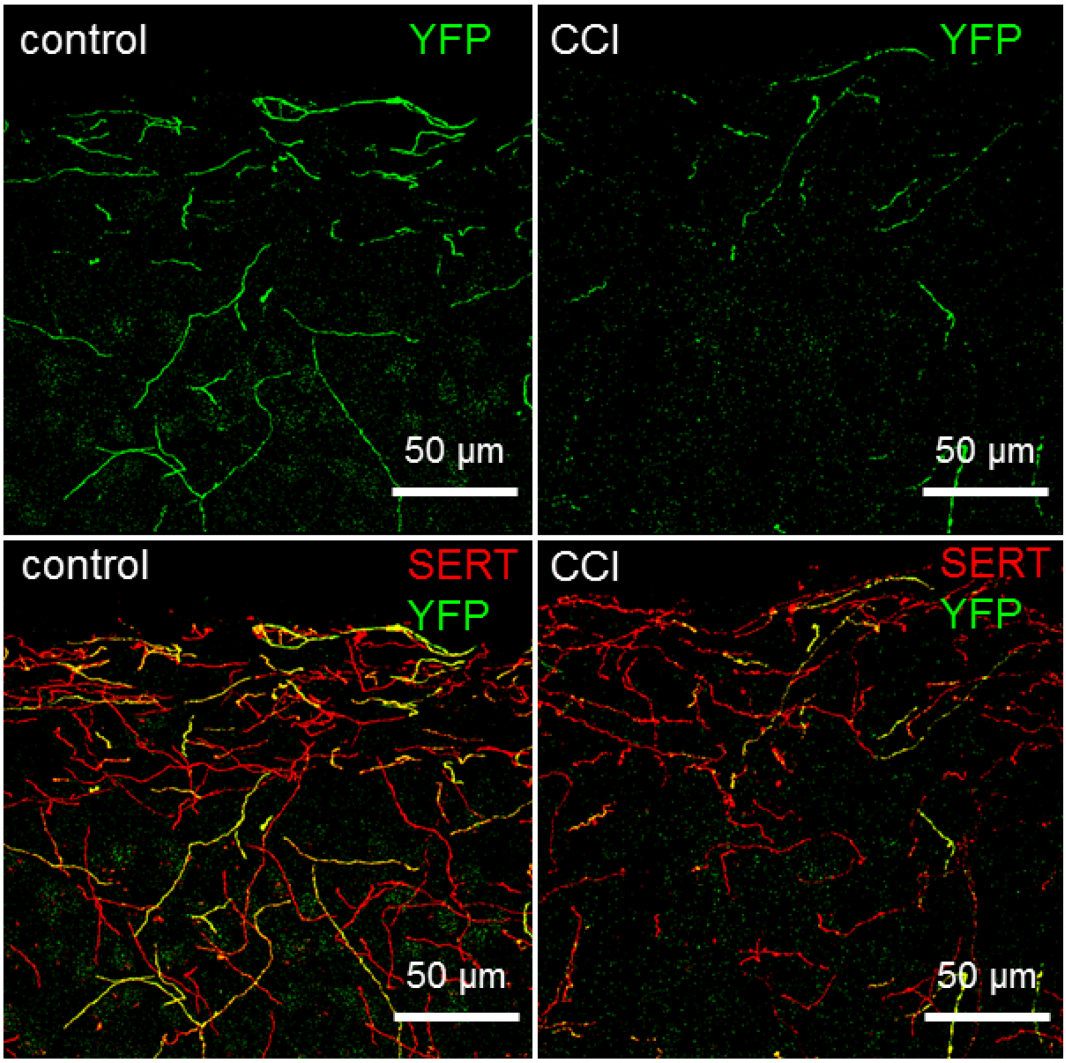

Figure 12. The apparent 5-HT fiber loss following CCI is not due to decreased SERT expression. Mice with YFP (top) constitutively expressed in a subset of dorsal raphe serotonergic neurons and their projections into the neocortex exhibit a similar degree of loss of YFP signal and SERT signal (bottom) in layer 1 posterior to injury, one week after CCI.

Reactive gliosis is not correlated with the degree of 5-HT fiber loss

One of the key features of the controlled cortical impact injury, especially as compared to an amphetamine lesion, is that it models common aspects of traumatic brain injury such as reactive gliosis secondary to injury. This is important as reactive gliosis is known to inhibit axonal growth (Yiu and He, 2006). We therefore wished to examine the scope and dynamics of reactive astrocytosis following controlled cortical impact and assess its relation to the degree of serotonin fiber loss and recovery.

To achieve this sagittal sections adjacent to those used for quantification of serotonin fiber density were processed with double-label immunohistochemistry (Figure 13) against NeuN to identify neocortical layers and against GFAP, which is expressed by reactive, but not resting, astrocytes (Eng and Ghirnikar, 1994).

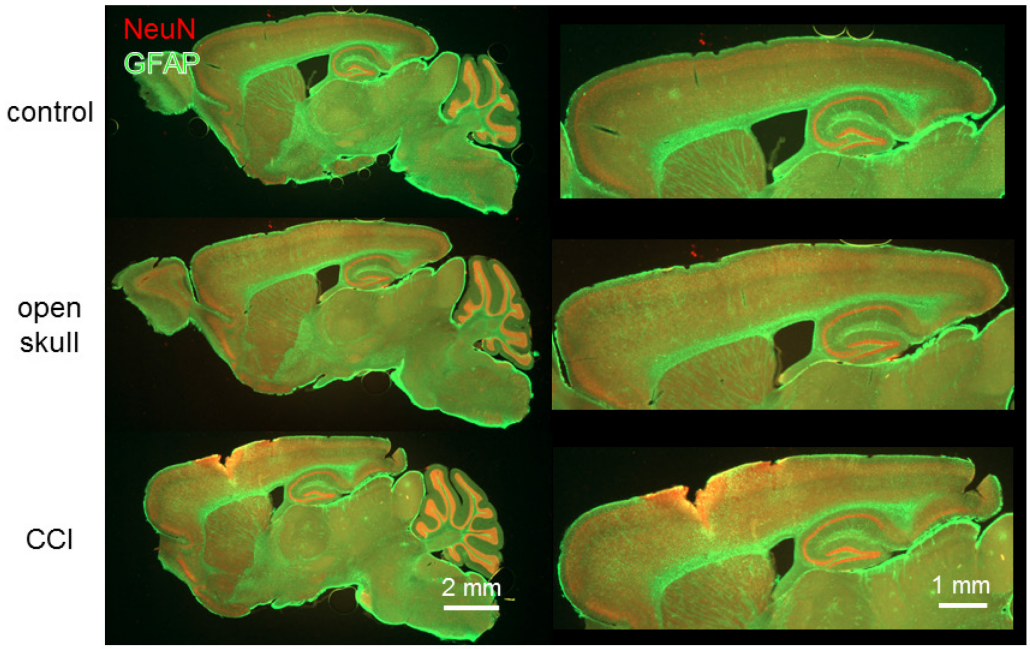

Figure 13. Low magnification exemplar images of GFAP immunohistochemistry reveals the extent of reactive gliosis evoked by CCI. The extent of reactive gliosis following open skull treatment (middle row) and CCI treatment (bottom row) compared to control tissue (top row) is evident in low magnification images (left column). Focusing on the neocortex at slightly higher magnification reveals few reactive astrocytes in control tissue, but a large number of reactive astrocytes in both the open skull and CCI tissue (right column).

In order to compare the level of reactive gliosis to the degree of serotonin fiber innervation, higher magnification (10x) single-photon confocal images were taken at the same anatomical locations as the images used for serotonin fiber density quantification.

The distinct morphology of the reactive astrocytes allows for accurate manual cell counting, which was performed for layer 1, 2/3 and 4 and expressed as cells per 100 μm^2.

These images (Figure 14) clearly reveal profound reactive gliosis across layers 1, 2/3, and 4 anterior to the injury site, one week post-surgery for both the open skull (layer 1: 7.7 ± .3, n = 4, $p < 0.001$; layer 2/3: 6.3 ± 1.4, n = 4, $p < 0.01$; layer 4: 3.9 ± 1.3, n = 4) and CCI groups (layer 1: 7.5 ± 0.4, n = 4, $p < 0.001$; layer 2/3: 9.1 ± 0.5, n = 4, $p < 0.001$; layer 4: 6.3 ± 0.1, n = 4, $p < 0.001$) compared to control tissue (layer 1: 1.7 ± 0.3, n = 4; layer 2/3: 0.2 ± 0.1, n = 4; layer 4: 0.2 ± 0.1, n = 4). This result was surprising based on the lack of significant serotonin fiber loss anterior to the injury site (Figure 7); we did not expect as much reactive astrogliosis in regions that had been spared from serotonin axon loss as in regions that had sustained significant serotonin fiber loss. Since the degree of reactive gliosis in layer 1 was similar between the open skull injury and CCI groups, as was the degree of serotonin axon loss, it suggests that the open craniotomy plays a large role in the injury model.

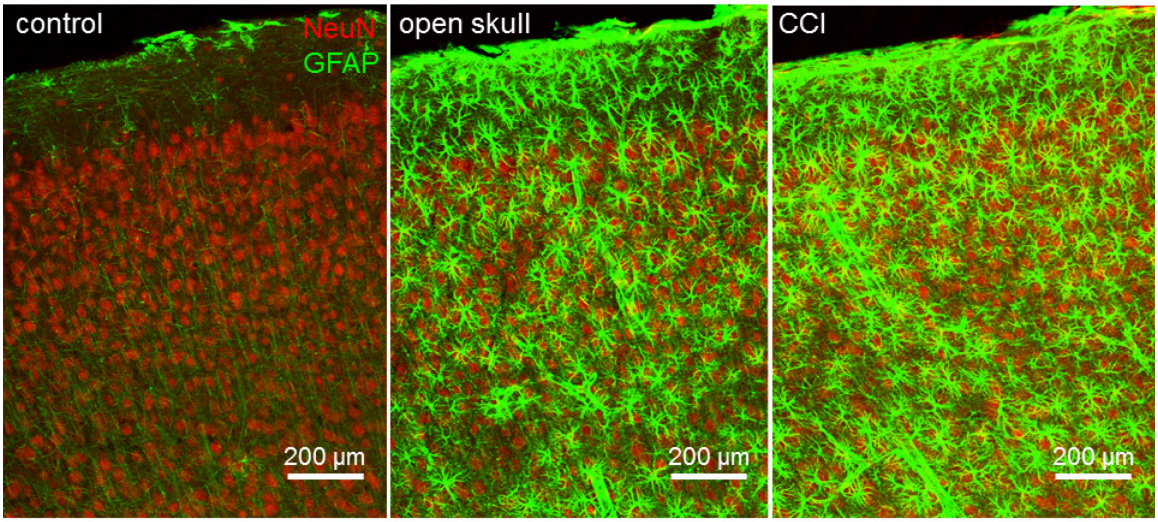

Figure 14. Exemplar images show reactive gliosis anterior to the CCI injury site, one week after surgery. Immunohistochemistry against GFAP reveals profound astrogliosis across all neocortical layers in both open skull (middle) and CCI (right) groups compared to control (left) tissue.

Three months post-surgery, the number of reactive astrocytes anterior to the injury site decreases to near-control levels (Figure 15). In the open skull group there was a significant decrease in the number of reactive astrocytes in layer 1 at three months (1.9 ± 0.5, $n = 4$, $p < 0.01$) compared to one week post-surgery. The same trend was observed in the CCI group (2.8 ± 0.7, $n = 4$, $p < 0.001$). Significant decreases were also observed in layer 2/3 (open skull: 0.7 ± 0.1, $n = 4$, $p < 0.001$; CCI: 1.9 ± 0.8, $n = 4$, $p < 0.05$) and layer 4 (open skull: 0.3 ± 0.05, $n = 4$, $p < 0.001$; CCI: 0.8 ± 0.1, $n = 4$, $p < 0.001$) at three months compared to one week post-surgery. The only significant difference that remained between groups three months post-surgery was the number of reactive astrocytes in the CCI group (0.8 ± 0.1, n

= 4, $p < 0.01$) in layer 4 anterior to the injury site compared to the control group (0.08 ± 0.08, n = 4).

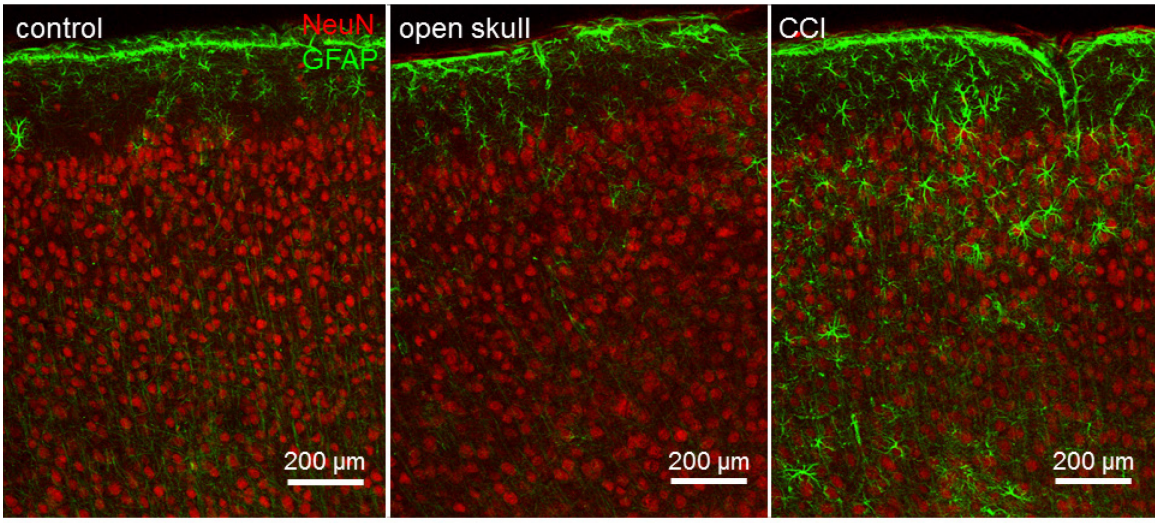

Figure 15. Exemplar images show reactive gliosis anterior to the CCI injury site, three months surgery. Immunohistochemistry reveals that three months post-surgery, astrogliosis across all neocortical layers in the open skull (middle) group has returned to control levels while some astrogliosis remains present in the CCI group (right) compared to control (left) tissue.

Quantification of reactive astrocyte number anterior to injury one month post-surgery reveals that an intermediate level of astrogliosis in layer 1, while astrogliosis in layers 2/3 and 4 has already resolved and looks similar to control levels (Figure 16). In summary, there is a profound amount of reactive gliosis anterior to craniotomy one week post-

surgery, which begins to resolve at one month, and no longer significantly persists at three months (t-tests, $p > 0.016$).

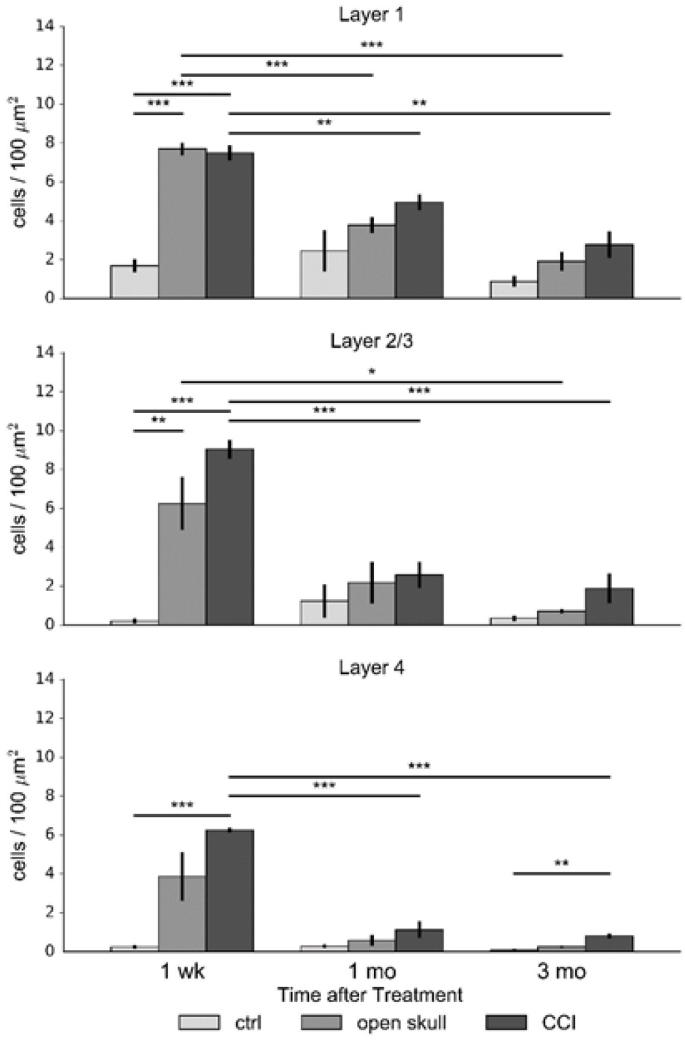

Figure 16. Quantification of reactive gliosis anterior to CCI injury site. The density of reactive astrocytes in both open skull and CCI groups one week following treatment is greatly increased. This increase is transient as there is a significant decrease in reactive astrocytes one month and three months post-surgery.

The reactive gliosis posterior to the injury site looks similar to that anterior to the injury site, when measured one week post-surgery (Figure 17). Both the open skull and CCI groups have significant increases in reactive astrocyte density in layer 1 (open skull: 7.4 ± 0.8, n = 4, $p < 0.01$; CCI: 8.1 ± 0.8, n = 4, $p < 0.01$) and layer 2/3 (open skull: 7.5 ± 1.7, n = 4, $p < 0.01$; CCI: 8.5 ± 1.3, n = 4, $p < 0.01$) compared to control levels (layer 1: 1.2 ± 0.2, n = 4; layer 2/3: 0.5 ± 0.2, n = 4). There is a trend toward increased reactive astrocyte gliosis in layer 4 as well, but due to large variability this is not statistically significant (control: 0.3 ± 0.2, n = 4; open skull: 5.0 ± 1.6, n = 4; CCI: 5.1 ± 1.8, n = 4; t-tests, $p > 0.016$).

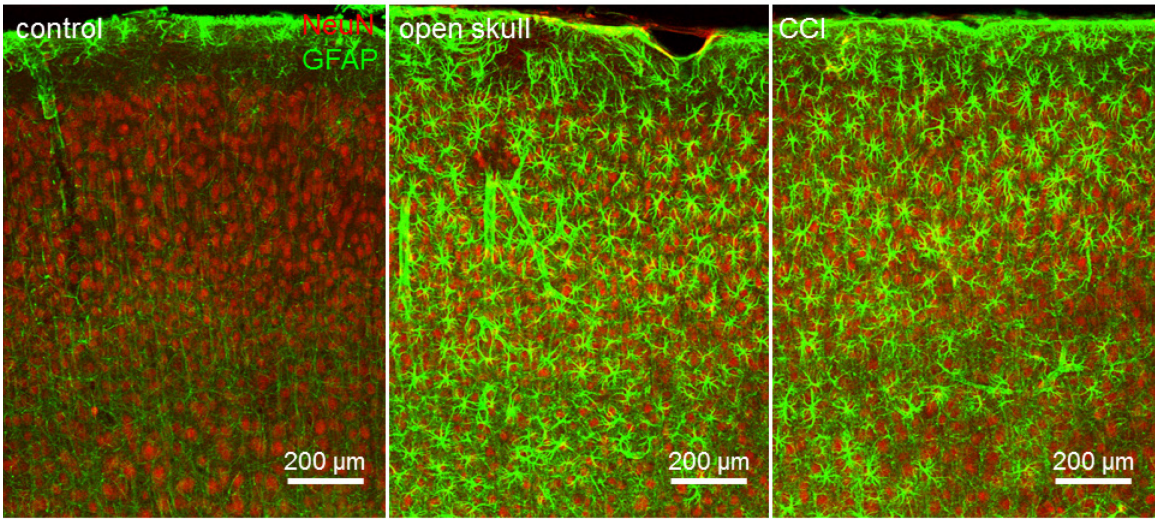

Figure 17. Exemplar images show reactive gliosis posterior to the CCI injury site, one week after surgery. Immunohistochemistry against GFAP shows a stark increase in reactive astrocytes one week post-surgery in both the open skull (middle) and CCI (right) groups compared to control tissue (left). This increase is evident in layers 1, 2/3, and 4.

Three months following injury there is a significant decrease in reactive gliosis compared to one week post-surgery in the open skull and CCI groups (Figure 18). There is no change in the control tissue. While it appears that there is a greater degree of persistence of astrogliosis in the CCI group compared to the control and open skull groups at three months post-surgery, this difference is not statistically significant.

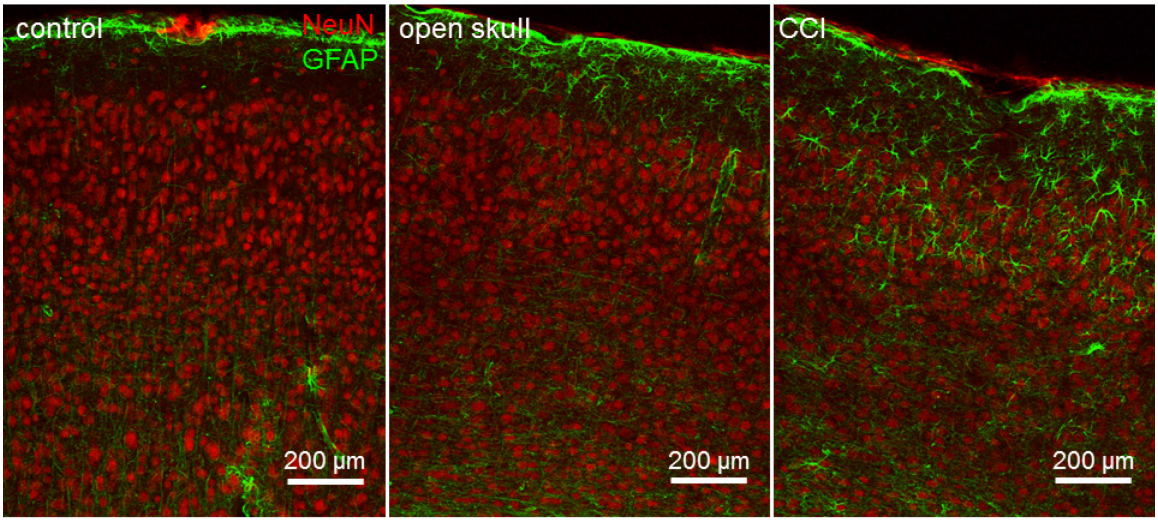

Figure 18. Exemplar images show reactive gliosis posterior to CCI injury site, three months after surgery. Reactive gliosis has almost completely resolved in the open skull group (middle) which looks similar to control tissue (left) three months post-surgery. Some remaining reactive astrocytes, especially in layers 1 and 2/3, are visible in the CCI group (right).

There are no differences between treatment groups in any measured neocortical layer at three months post-surgery (Figure 19). In layer 1 posterior to the injury site, reactive gliosis in both the open skull (1.7 ± 0.3, n = 4, $p < 0.01$) and CCI (3.0 ± 0.9, n = 4, $p < 0.01$) groups is significantly lower than it was at one week post-surgery. The same holds true for layer 2/3 (open skull: 0.4 ± 0.04, n = 4, $p < 0.05$; CCI: 1.4 ± 0.7, n = 4, $p < 0.01$).

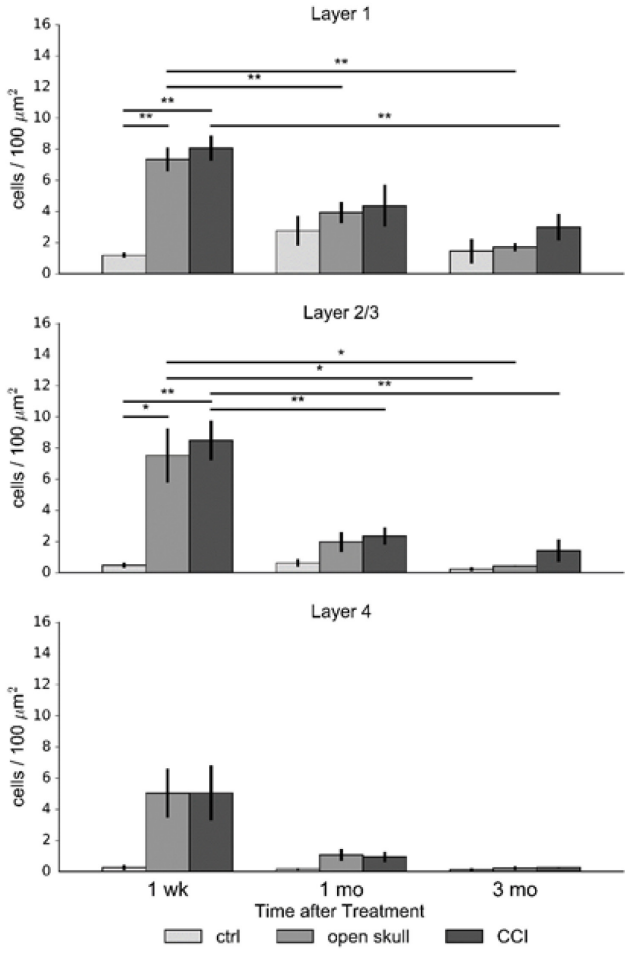

Figure 19. Quantification of reactive gliosis posterior to CCI injury site. There is a stark increase in reactive astrocyte density across all layers of neocortex when measured one week post-surgery in the open skull and CCI groups. The astrogliosis begins to

significantly resolve at one month, and there is no difference between treatment groups in any layer at three months post-surgery.

Next we asked whether the degree of reactive gliosis was correlated with the degree of serotonin fiber loss following injury. To answer this, reactive gliosis and serotonin innervation data were combined for each animal. This yields data points that each have an anatomical location, treatment group, time point, reactive astrocyte density, and serotonin fiber density. Data points missing any of these values due to tissue processing were discarded from further analysis. GFAP positive cell density was then plotted against normalized serotonin fiber density for all treatment groups, time points, and anatomical locations (Figure 20A). We found that this resulted in a significant relationship between the reactive gliosis and serotonin fiber density using the Pearson correlation (correlation: -0.3895, $p < 0.001$). However, this correlation is trivial: it is skewed by control tissue at all time points, where the normalized serotonin fiber density is 100% and only rare reactive astrocytes are present. To a lesser degree, this correlation also reflects the fact that reactive gliosis resolves as serotonin fiber regrowth is observed.

To more accurately address whether reactive gliosis is correlated with serotonin fiber damage we restricted this analysis to only include the CCI group one week post-surgery (Figure 20B). In this data subset there is no significant relationship (Pearson correlation, $p > 0.05$) between the two variables, a finding that reflects that even profound reactive

gliosis is not indicative of serotonin fiber damage. In other words, profound reactive gliosis was found both anterior and posterior to the CCI injury, but only the posterior site showed significant loss of serotonin fibers. Furthermore, when analysis is restricted to the layer 1 and the CCI group, astrogliosis still fails to predict the degree of serotonin fiber loss.

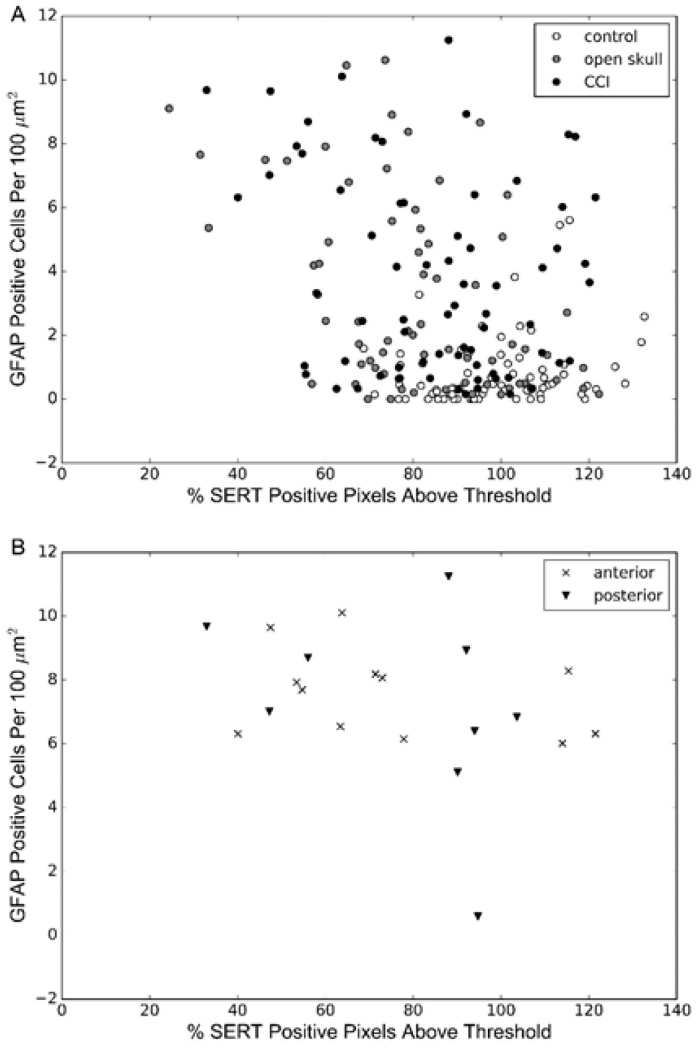

Figure 20. Scatterplots show the relationship between reactive gliosis and 5-HT fiber loss. A) All time points and treatment groups are plotted together and reveal a correlation between reactive gliosis and serotonin fiber density that is primarily a result of control data with high serotonin fiber density and low reactive astrocyte density. Control group (open circles), open skull group (gray circles), and the CCI group (black circles) are denoted. B) There is no significant relationship between the variables when only

considering the CCI group one week post-surgery. X denotes anterior regions, triangle denotes posterior regions.

Microglial density is not correlated with the degree 5-HT fiber loss

The response to traumatic brain injury also contains an inflammatory component. Microglia are an important inflammatory cell in the neocortex (Dheen et al., 2007) and have been shown to rapidly respond to brain injury (Davalos et al., 2005; Szalay et al., 2016). Therefore we sought to determine whether there was a change in microglial density following controlled cortical impact as well as whether there was a relationship between microglial density and serotonin fiber loss.

To visualize and quantify microglia we utilized double-label immunohistochemistry against Iba1, which is expressed only by microglia in the neocortex (Ito et al., 1998), and NeuN to identify neocortical layers on sagittal sections adjacent to those used for quantification of serotonin fiber density. Anatomical regions matching those used for the previous analysis were imaged under a 20x 0.8 N.A. objective with single-photon confocal microscopy. In order to capture all of the layers of interest, two dorso-ventral adjacent 10 μm confocal stacks were captured, maximally projected, and stitched together. The Iba1 signal was contrast enhanced using the iterative threshold algorithm described above to isolate microglia from background signal. Microglial density was calculated as the percent of total pixels in the layer of interest that were positive for Iba1 signal.

One week post-surgery there was no significant difference (t-tests, $p > 0.016$) in microglial density between treatment groups anterior to the injury site in layer 1 (control: 100.0 ± 12.8%, n = 4; open skull: 88.4 ± 7.1%, n = 4; CCI: 123.1 ± 17.4%, n = 4), layer 2/3 (control: 100.0 ± 9.9%, n = 4; open skull: 96.1 ± 4.3%, n = 4; CCI: 99.9 ± 13.1%, n = 4), or layer 4 (control: 100.0 ± 10.9%, n = 4; open skull: 72.4 ± 3.9%, n = 4; CCI: 87.1 ± 11.7%, n = 4) (Figure 21).

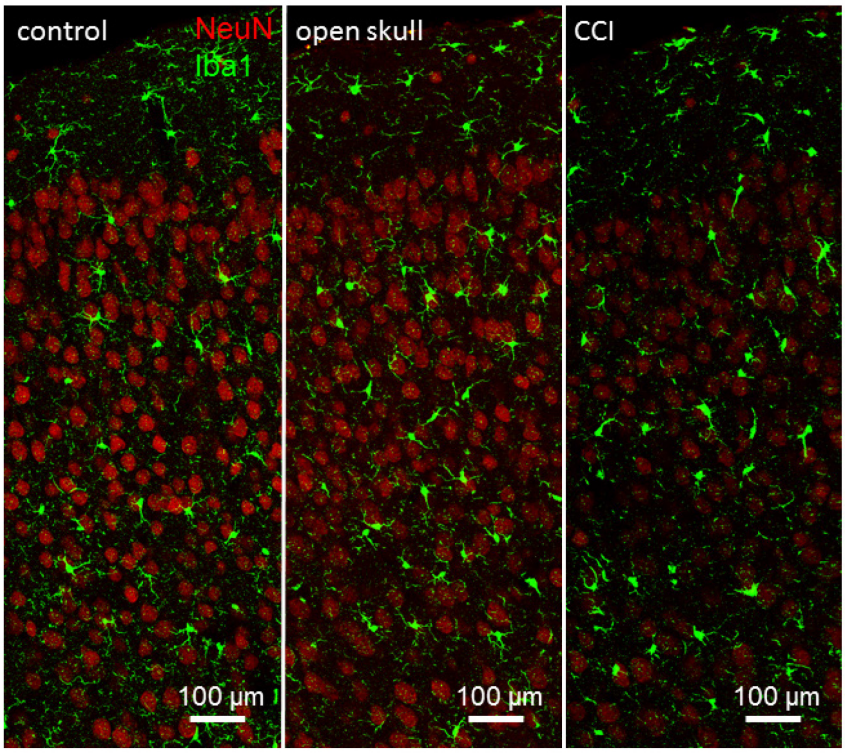

Figure 21. Exemplar images of Iba1 immunohistochemistry show microglia anterior to the CCI injury site, one week after surgery. There does not appear to be an increase in microglial density one week post-surgery in neocortical layers 1, 2/3, or 4 in open skull (middle) or CCI (right) groups compared to control tissue (left).

Microglial density remained constant anterior to the injury site throughout the experimental time points (Figure 22). While a there is a trend toward increased microglial density in layer 1 compared to control density at one week, one month, and three months post-surgery, there were no statistical differences in the groups, likely a result of high variability of microglia visible between samples. Microglia activation secondary to injury leads to morphological changes including increased soma size and shortened processes (Cho et al., 2006). Analysis to determine whether these shape changes are present anterior or posterior to the injury site following controlled cortical impact is ongoing.

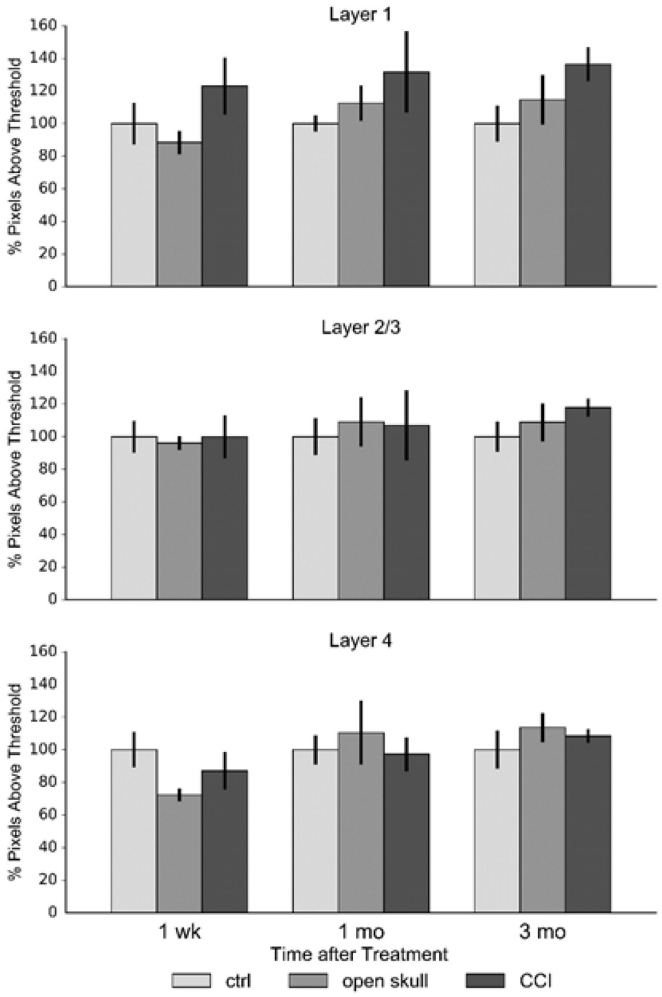

Figure 22. Quantification of microglial density anterior to the CCI injury site. There are no differences in microglia density between control, open skull, and CCI treatments at any of the time points measured.

As with the anterior to injury region, there were no microglia density differences between treatment groups posterior to the injury site one week post-surgery (Figure 23). Microglia density for the open skull (layer 1: 92.5 ± 14.2%, n = 4; layer 2/3: 89.7 ± 4.7%, n = 4; layer 4: 92.8 ± 4.5%, n = 4) and CCI (layer 1: 111.4 ± 24.6%, n = 4; layer 2/3: 103.4 ± 8.3%, n = 4; layer

4: 94.5 ± 7.1%, n = 4) groups was comparable to control levels (layer 1: 100.0 ± 16.0, n = 4; layer 2/3: 100.0 ± 11.0%, n = 4; layer 4: 100.0 ± 11.3%, n = 4) in layers 1, 2/3, and 4.

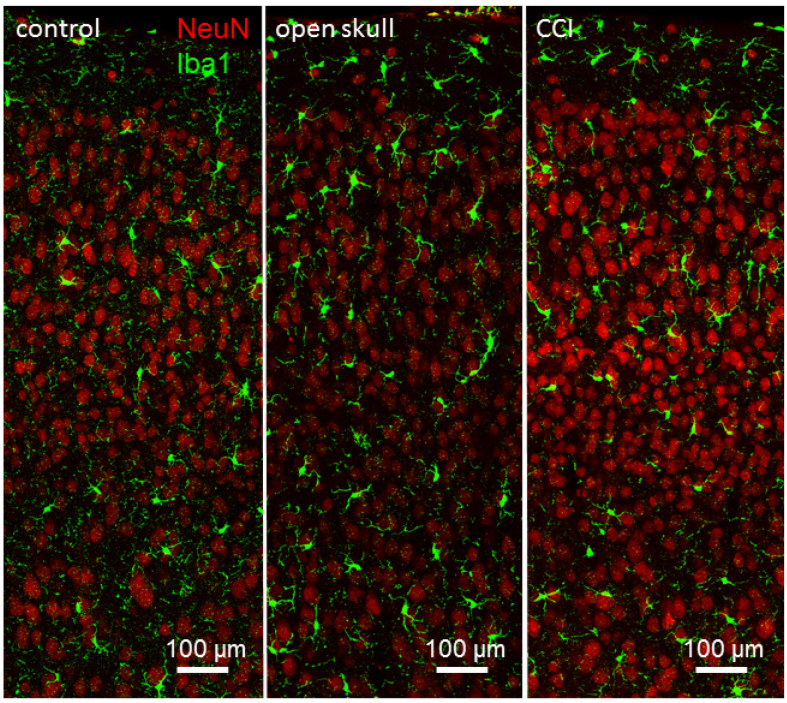

Figure 23. Exemplar images of Iba1 immunohistochemistry show microglia posterior to CCI injury site, one week after surgery. There are no significant differences in microglia density one week post-surgery posterior to injury in neocortical layers 1, 2/3, or 4.

When we quantified microglial density posterior to the injury site at later time points (one month and three months post-surgery) we also did not observe any significant changes between groups or across time points (Figure 24).

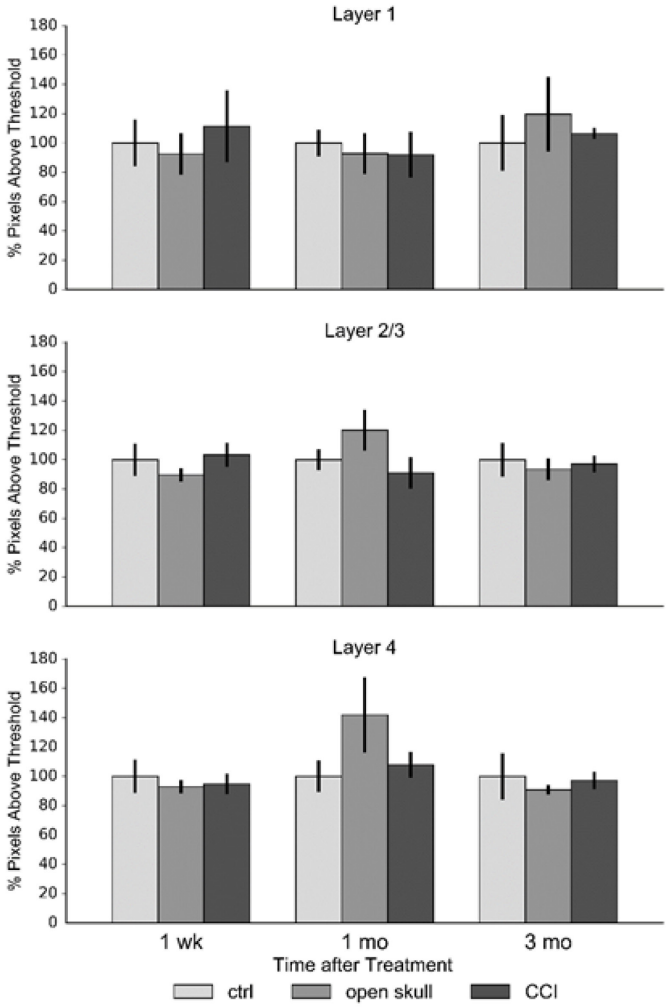

Figure 24. Quantification of microglial density posterior to CCI injury site. There were no significant differences in microglial density posterior to the injury site observed in layers 1, 2/3, or 4 among the treatment groups for any of the observed experimental time points.

Finally we asked if, even though there were no clear increases in microglial density following injury, there was a relationship between serotonin fiber loss and microglial density. This could suggest that either serotonin fiber damage, or related processes, attract

microglia to the damaged area or that an increase in microglia and related inflammatory processes could lead to exacerbation of serotonin fiber damage.

The same approach used to analyze the relationship between reactive astrogliosis and serotonin fiber density was used. When visualizing data for all of the treatment groups and experimental time points together, we did not observe a correlation between microglial density and serotonin fiber density (Figure 25A). This was in contrast to a significant relationship seen at this level between reactive gliosis and serotonin fiber density. This is because while there are very few reactive astrocytes in control tissue, or injured tissue at late time points, microglia are always present, both in healthy and injured tissue.

To see if controlled cortical impact injury affected microglial density, we looked only at the subset of data from the CCI group one-week post injury (Figure 25B). There was no significant relationship (Pearson correlation, $p > 0.05$) between microglial density and serotonin fiber density in this data subset.

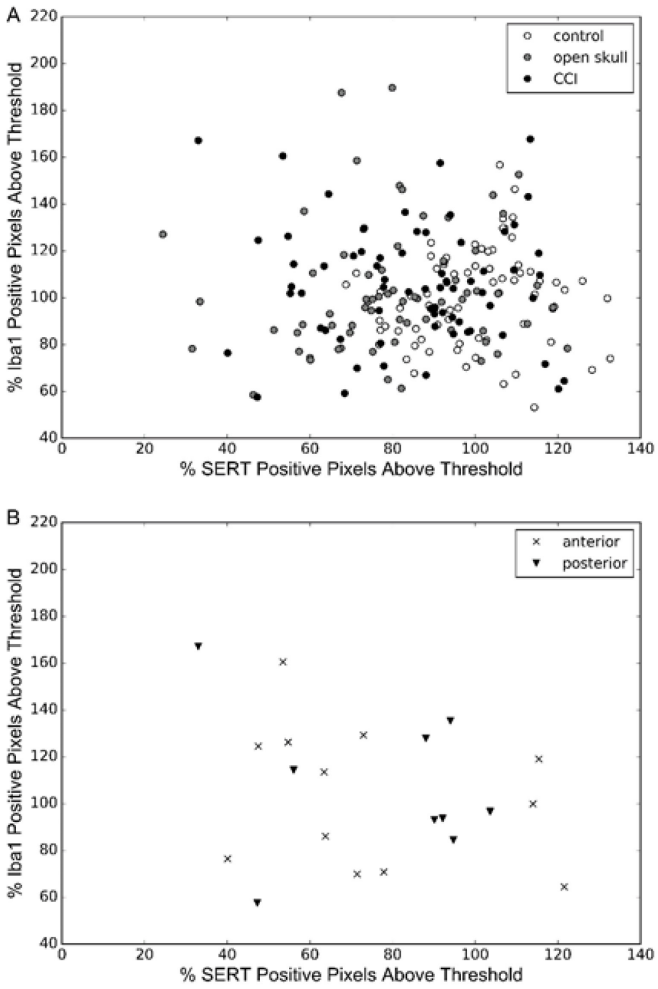

Figure 25. Scatterplots show the relationship between microglial density and 5-HT fiber loss. A) Plotting microglial density against serotonin fiber density for all treatment groups and time points does not reveal a relationship between the two measures. Control group (open circles), open skull group (gray circles), and CCI group (black circles) are denoted. B) There is also no significant relationship between the variables when only considering the CCI group one week post-surgery. X denotes anterior regions, triangle denotes posterior regions.

Conclusion

Traumatic brain injury, either from an open craniotomy alone or CCI, leads to significant serotonin fiber loss posterior to the impact region while sparing axons anterior to the impact region as observed one week post-surgery. This effect is greatest in layer 1 of the neocortex. This apparent fiber loss in not an artifact of reduced SERT expression as indicated by experiments using YFP expressed in SERT-positive neurons under the control of a constitutively-active viral promoter. Regrowth of serotonin fibers is observed at one month and three months post-surgery posterior to the impact region. There is profound reactive gliosis present one week post-surgery that begins to resolve at one month and returns to control levels three months post-surgery. However, the degree of reactive gliosis is not correlated with the degree of serotonin fiber loss in the CCI group. Microglial density does not appear to change in response to open skull or CCI injuries, and is not correlated to the degree of serotonin fiber density loss in the CCI group.

Chapter 4: Repetitive Mild Traumatic Brain Injury and 5-HT Fiber Innervation

In recent years there has been growing evidence that repetitive mild traumatic brain injury (rmTBI), such as repeated concussions sustained during sports activity, can lead to emotional, physical, and cognitive defects months and years after injury, collectively termed post-concussive syndrome (Williams et al., 2010). The emotional features of post-concussive syndrome include irritability, anxiety, and depression, which could be a clinical manifestation of damage to serotonergic innervation of the neocortex (as well as other brain regions). To test this possibility we exposed mice to an rmTBI model and quantified serotonin fiber density in multiple regions of neocortex. This work was done in collaboration with Drs. Leyan Xu and Vasillis Koliastsos.

rmTBI does not lead to decreased 5-HT fiber innervation in neocortex

Mice were exposed to a closed-skull, non-contusive, impact acceleration injury that mimics the biomechanics of concussion inducing impacts (Xu et al., 2016). We began with a pilot study to assess whether there is a graded effect of the injury, with mice receiving either no impacts (sham group), a single impact (1x group), one impact per day on four days spaced over a week (4x group), or two impacts a day spaced over a week (8x group). Animals with visible fractures of the skull following any of the hits were sacrificed

immediately and excluded from analysis. Note that sham group in these experiments therefore receives no treatment as this model does not utilize a craniotomy, unlike the open skull condition in the controlled cortical impact model. Mice were allowed to recover for one week after the last day of impacts and were then sacrificed.

Double-label immunohistochemistry against SERT to visualize serotonin fibers and NeuN to identify neocortical layers was performed on sagittal sections of the left hemisphere (Lateral 0.60 mm; chosen to be near the midline, but before the cortex begins curving toward the medial longitudinal fissure). Because the biomechanics of the injury can lead to dissimilar forces on different anatomical areas, we imaged both motor and somatosensory cortex using single-photon microscopy. The imaging z-stacks were maximally projected and the SERT signal was contrast enhanced using an iterative thresholding algorithm. Serotonin fiber density was measured as the percent of all pixels in the neocortical layer of interest that were positive for thresholded SERT signal.

In layer 1 of motor cortex there was no significant difference (t-tests, $p > 0.0125$) in serotonin fiber density between the sham (18.0 ± 3.2%, n = 3), 1x impact (21.0 ± 6.4%, n = 3), 4x impact (19.8 ± 3.9%, n = 4), and 8x impact (22.0 ± 4.0%, n = 2) groups (Figure 26). In addition, there was no gross anatomical distortion of the tissue or evidence of necrosis based on the fact that NeuN positive neuronal cell bodies have well defined borders in all of the injury groups.

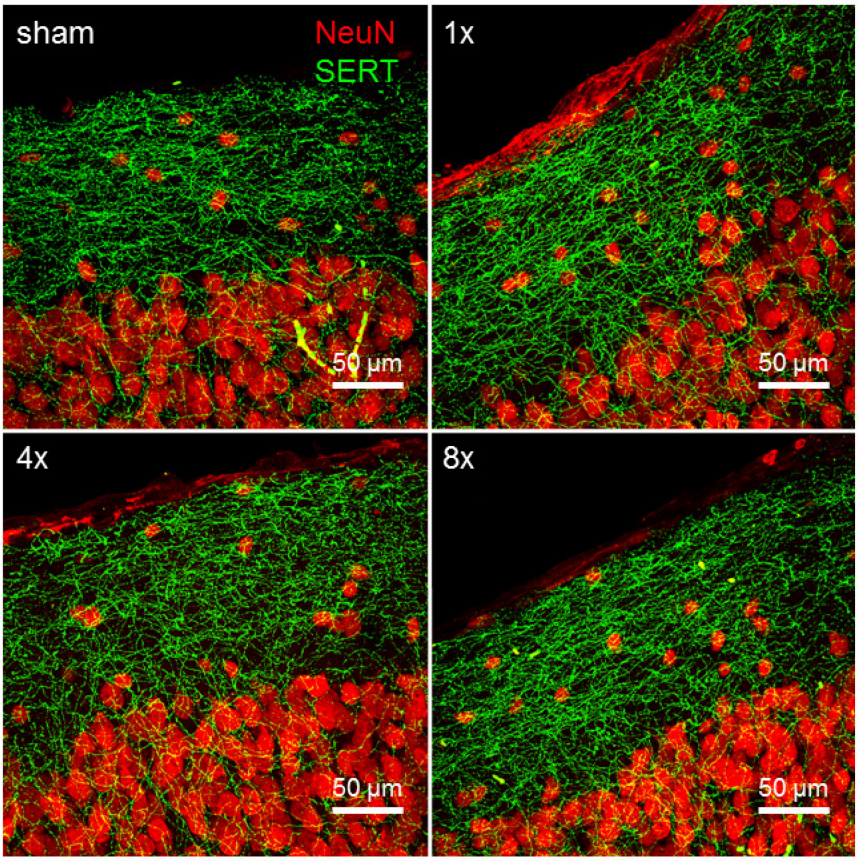

Figure 26. Exemplar images show 5-HT fiber innervation in motor cortex following repetitive mild TBI. Serotonin fiber density appears similar one week after impacts in the 1x impact, 4x impact, and 8x impact groups compared to tissue from sham treated control animals.

We also quantified serotonin fiber density in layers 2/3 and 4 in motor cortex, but did not observe any differences in innervation among these groups (Figure 27).

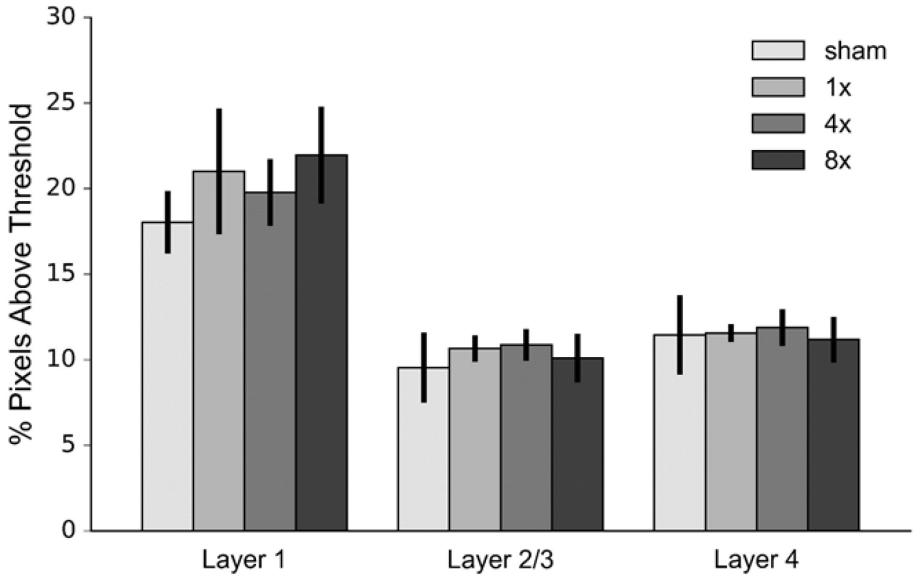

Figure 27. Quantification of 5-HT fibers in motor cortex from a repetitive mild TBI (rmTBI) pilot study. There were no differences in serotonin fiber density following rmTBI across a range of injury severity. Layer 1 had a greater density of serotonin fibers than deeper cortical layers, which reflects the normal serotonin fiber innervation pattern in adult mouse neocortex. Sample size is as follows: sham n = 3, 1x n = 4, 4x n = 4, 8x n = 2.

It is possible that fibers in motor cortex were spared because they were anterior to the area above which the impact was made. We therefore also measured serotonin fiber density in the somatosensory cortex which lies directly underneath the area of the skull that was impacted. However, we still did not observe differences in serotonin fiber innervation in layer 1 among the treatment groups (sham: 12.6 ± 4.5%, n = 3; 1x: 16.9 ± 2.1%, n = 3; 4x: 12.7 ± 4.5%, n = 4; 8x: 15.2 ± 0.5%, n = 2) (Figure 28). As in the motor cortex, there was no evidence of gross tissue damage in this region.

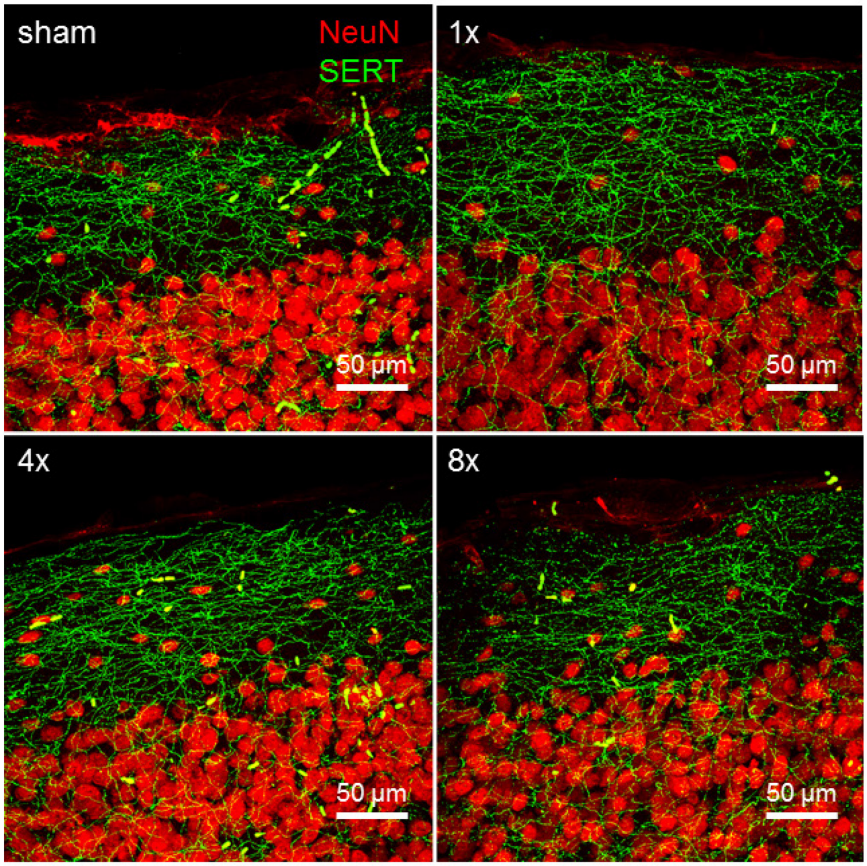

Figure 28. Exemplar images show 5-HT fiber innervation in somatosensory cortex following repetitive mild TBI. Serotonin fiber density in layer 1 of the sham-treated somatosensory cortex is lower than in the sham-treated motor cortex due to the normal antero-posterior distribution of serotonin fibers. However, there is no difference in serotonin fiber density between the treatment groups in layer 1 of somatosensory cortex.

We also measured the serotonin fiber density in layers 2/3 and 4 of somatosensory cortex, but again saw no differences in innervation (Figure 29).

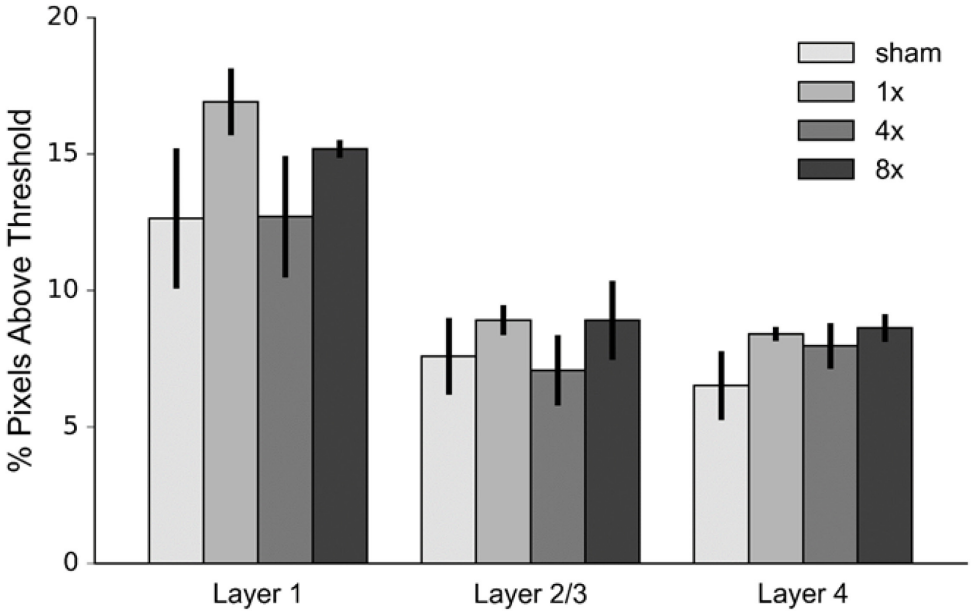

Figure 29. Quantification of 5-HT fibers in somatosensory cortex from a repetitive mild TBI (rmTBI) pilot study. There were no differences in serotonin fiber density between treatment groups in the somatosensory cortex. Innervation was quantified in layer 1, 2/3, and 4. Sample size is as follows: sham n = 3, 1x n = 4, 4x n = 4, 8x n = 2.

While there was no evidence of rmTBI leading to serotonin fiber loss in the pilot data, the possibility remained that we were missing an effect due to small sample size. We therefore repeated the experiment (sham and 8x impact groups, only) on a larger population of mice. Data from the pilot experiment was normalized to the average innervation density of the sham group for each region. Data from the additional experiment was normalized the same way using internal sham control images that were processed together. The normalized data sets were then combined and averaged. There was no difference

observed between sham (n = 9) and 8x impact (n = 7) groups in layers 1, 2/3, or 4 in either motor or somatosensory cortex (Figure 30).

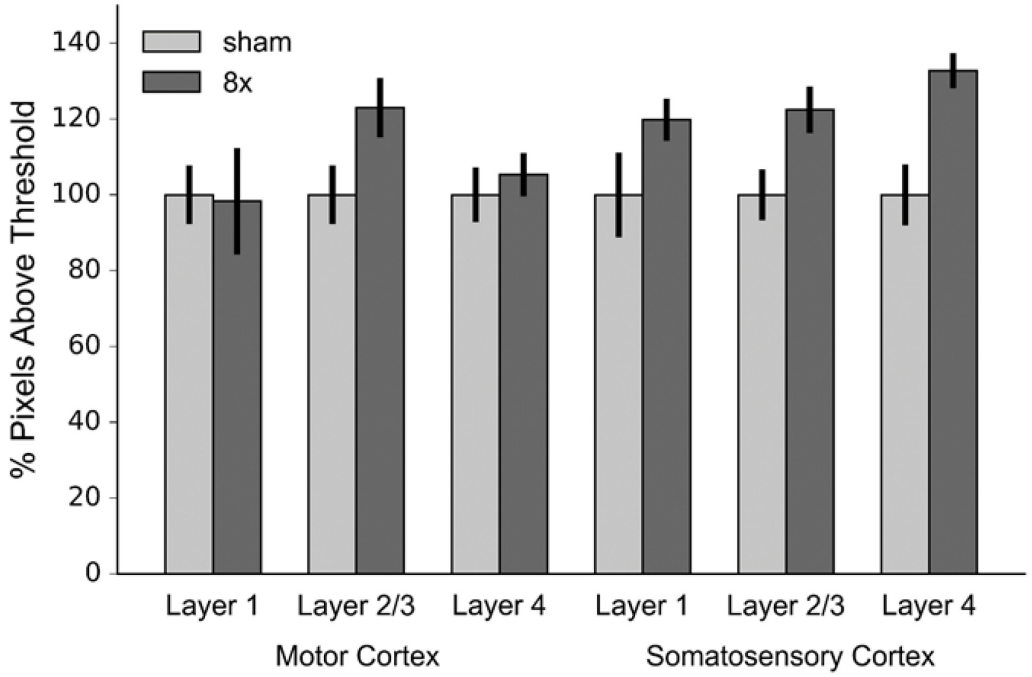

Figure 30. Quantification of 5-HT fiber innervation in motor and somatosensory cortex following repetitive mild TBI. Expanding the sample size of the sham and 8x impact groups did not reveal an effect of repetitive mild traumatic brain injury on serotonin fiber density in either motor or somatosensory cortex, in any of the neocortical layers analyzed. Sample size is as follows: sham n = 9, 8x n = 7.

rmTBI does lead to reactive gliosis in the optic tract

Another possibility is that, for an unidentified reason, the impact surgeries were unsuccessful and did not produce the type of force expected for this model. This rmTBI

model has been found to produce diffuse axonal damage and neuroinflammation in the optic tract under the same conditions as the present study (Xu et al., 2016). Therefore we turned to the optic tract to determine whether the injuries were similar to those previously reported.

Immunohistochemistry against GFAP to identify reactive astrocytes was performed and the optic tract of sham treated and 8x impact tissue was imaged using single-photon confocal microscopy. Sagittal slices from a single sham and 8x animal were used. The lateral plane of the sagittal slices was matched to that used for serotonin fiber density imaging. The confocal z-stacks were maximally projected and the GFAP signal was contrast enhanced using an iterative thresholding algorithm. We observed an obvious subjective increase in reactive astrocytes in the optic tract of tissue from the 8x impact group compared to tissue from sham treated animals (Figure 31). This confirmed that the impact injuries were performed successfully and produced effects in line with expectations of the model, which also reported an increase in GFAP expression in the optic tract.

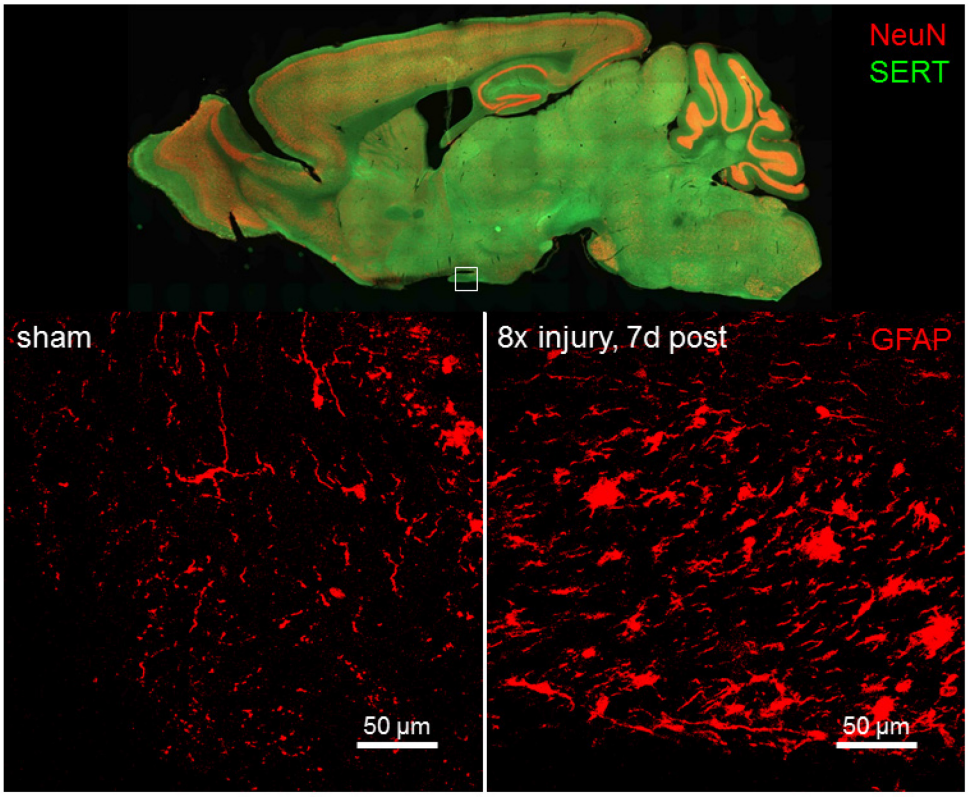

Figure 31. Exemplar images show reactive gliosis in the optic tract following repetitive mild TBI. Immunohistochemistry against GFAP reveals an increase in reactive astrocytes in the optic tract of tissue from the 8x impact group (bottom right) compared to tissue from the sham treated group (bottom left). A low magnification mosaic image (top) shows the location of confocal imaging (white box).

Conclusion

We hypothesized that repetitive mild traumatic brain injury would result in graded damage to neocortical serotonin fibers as the number of impacts was increased. However, we did not observe a difference in serotonin fiber density between control sham-treated

animals and any of the impact conditions. We confirmed that this was not do to a failure of the impacts to elicit injury as we replicated the reactive gliosis in the optic tract in the impact treated animals as previously reported (Xu et al., 2016).

Chapter 5: General Discussion

The purpose of these studies was to investigate whether there is a loss of serotonin fibers in mouse neocortex following traumatic brain injury, and if so, whether serotonin fibers are able to regrow to innervate the injured tissue. We found that following traumatic brain injury, either from CCI or an open skull injury, serotonin fiber density is decreased posterior (distal; Figures 8 and 10) but not anterior (proximal; Figures 5 and 7) to the impact when measured in layer 1 at one week post-surgery, and serotonin fibers are capable of regrowing into the injured area by one month post-surgery (Figure 11). Traumatic brain injury in this model was associated with significant reactive gliosis both anterior (Figures 14-16) and posterior (Figures 17-19) to the impact, but the level of reactive gliosis was not correlated with serotonin fiber density when measured 1 week after injury (Figure 20). Microglia are involved in the neuroinflammatory response to injury but there was no increase in density of these cells in injured or surrounding areas (Figures 21-24). We failed to see serotonin fiber loss in an established repetitive mild traumatic brain injury model (Figures 26-30; Xu et al., 2016), despite observing hallmarks of injury in the optic tract (Figure 31).

Limitations of the experimental models

The controlled cortical impact model of traumatic brain injury is highly reproducible, but one major disadvantage is the reliance of the model on a craniotomy over the impact site.

In the present study the craniotomy was left open, covered only by skin closed with a wound clip, before mice were returned to group housing. Under these conditions there was an unexpectedly large reactive gliosis response (Figure 17) as well as an unexpectedly large amount of serotonin fiber loss (Figure 8) in the open skull group compared to control animals that did not receive a craniotomy. There are several potential mechanisms by which serotonin fibers could have been damaged in this group. One likely explanation is that normal behavior such as social grooming or scratching at the wound site could result in damage to the tissue. While there was generally no gross deformity to the brain tissue under the craniotomy in these animals (Figure 4), this does not preclude a lighter insult from having selectively damaged certain fibers or structures in the area. Another possibility is that temperature dysregulation as a result of the craniotomy, which can lower brain temperature as much as 10 °C below core body temperature, either directly or indirectly leads to damage of serotonin fibers (Kalmbach and Waters, 2012). Regardless of the precise mechanism, however, this finding reinforces the importance of considering the craniotomy itself as an aspect of the injury when interpreting results from controlled cortical impact experiments.

Another surprising finding was the lack of serotonin fiber loss in deeper neocortical layers posterior to the impact site (Figure 10). Despite a reactive gliosis response in layers 1, 2/3, and 4, there was only significant fiber loss after controlled cortical impact in layer 1. The most straightforward explanation relies on the fact that deeper neocortical layers are

innervated by projections from the dorsal raphe, the fibers of which course anterior to posterior in deeper cortical layers with branches extending to innervate layers 2/3 and 4. These fibers could have been spared the full force of the controlled cortical impact while fibers from the median raphe which preferentially course in and innervate layer 1 were transected (or at least strongly compressed) by the impact, resulting in the observed decrease there.

While there was significant regrowth of serotonin fibers from one week post-surgery to one month post-surgery, there was not a further significant increase in serotonin fiber density between one month and three months post-surgery (Figure 11). There are two non-mutually exclusive explanations. The first is that there is a physiological limit to the amount of regrowth that serotonin fibers are capable of after injury and that this limit is reached by or soon after the one month time point. The second is that the plateau in regrowth between one month and three months reflects a dynamic equilibrium between two effects: serotonin fiber regrowth and progressive atrophy of surviving or new serotonin fibers. It has been shown that traumatic brain injury is a progressive degenerative process, with neuronal death persisting at least one year following a traumatic brain injury in rat (Smith et al., 1997). Therefore it is possible that secondary effects of injury are masking continuing regrowth between one and three months post-surgery.

It was recently reported that SERT expression decreases 7 days after controlled cortical impact injury in mice as measured by mRNA expression via real-time PCR and protein levels via western blotting (Abe et al., 2016). The authors also noted that, while not significant, there seemed to be a rebound in SERT expression 14 days post-surgery. Based on this data they concluded that damaged serotonin fibers decreased expression of SERT, but that this damage was not irreversible. Our current data suggest that this interpretation is incomplete. We confirm that SERT expression is decreased following controlled cortical impact, but also show that this is in fact due to serotonin fiber degeneration as measured by loss of serotonin fibers labeled with YFP that is not dependent on SERT expression (Figure 12). The increase in SERT expression described by the authors at 14 days post-surgery, then, could in fact be early regrowth of serotonin fibers into the injured area.

We had hypothesized that repetitive mild traumatic brain injury would also result in damage to serotonin fibers. However, we did not see a decrease in serotonin fiber innervation using our methodology across a range of repetitive mild traumatic brain injury severity (Figures 27 and 29). This negative finding is not a result of these injuries being too mild. The strength of the impact can be appreciated by the need to manually resuscitate mice following injury. Repeated impacts lead to diffuse axonal damage in certain white matter tracts, degeneration of axons in the optic nerve and tract, and a neuroinflammatory response evidenced by microglia activation and reactive astrogliosis (Xu et al., 2016). Consistent with these published findings, we also observed reactive

astrogliosis in the optic tract (Figure 31). Our findings should not be taken as conclusive evidence against serotonin fiber damage as a result of repetitive mild traumatic brain injury, however. It is possible that there exist functional deficits in the serotonergic system as a result of injuries from this model that are not reflected in a serotonin fiber density measure. It is also possible that while this model does not produce damage to serotonin fibers, other models of mild traumatic brain injury may reveal that this causal link does exist under some conditions.

Implications for human traumatic brain injury

One of the issues facing clinical treatment of traumatic brain injury is that promising preclinical studies have failed at the clinical trial stage (Xiong et al., 2013). This is a consequence of the heterogeneity of traumatic brain injuries that present in the clinic. Therapies that are developed and found to be successful in one animal model may not be effective in other animal models or across diverse injuries in the clinic. Our findings of serotonin fiber loss in one traumatic brain injury model but not another help highlight this issue. We need to continue to develop models that complement each other and the use of multiple models moving forward will be important. Different impact models may yield different results, but by using the strengths of individual models and not overgeneralizing between models, this should serve to advance our understanding of the mechanisms underlying traumatic brain injury and its associated cognitive defects.

Controlled cortical impact (CCI) creates a reproducible injury that is pathologically similar to human traumatic brain injury (TBI) across a range of insult strength. Mild severity injuries lead to axonal damage in the subcortical white matter, while moderate severity injuries induce extensive damage to both cortical and subcortical fibers (Fox et al., 1998). Both mild and moderate injuries lead to long-lasting fine motor coordination deficits. Severe CCI can lead to prolonged (up to 36 hour) coma with axonal injury visible in subcortical white matter, the thalamus, and the midbrain (Lighthall et al., 1990). In line with differences in axonal damage, the severity of TBI dictates the degree of behavioral deficits (Yu et al., 2009). CCI injury is also accompanied by degeneration of neurons in cortex adjacent to site of injury, as well as the ipsilateral hippocampus and dentate gyrus (Smith et al., 1995). There is also evidence from acute slice recordings that loss of inhibitory interneurons in the cortex following CCI results in increased cortical excitability and glutamatergic signaling (Cantu et al., 2015). Data on damage to specific axonal fiber types following controlled cortical impact is lacking.

The fact that serotonin fibers are damaged by controlled cortical impact or the open skull treatment, and that serotonin fibers are able to reinnervate injured areas provides an important insight into the potential biological basis behind certain outcomes secondary to traumatic brain injury, such as depression. Loss of serotonin fibers reinforces the importance of treating traumatic brain injury as a disease process rather than a distinct injury event; even if the immediate effects of an injury resolve, there is the potential for

continued dysfunction of a major neuromodulatory system in the neocortex. This new evidence also serves as an important target for potential therapies that either serve to decrease serotonin fiber loss following injury or aid in increasing the rate or degree of reinnervation in injured areas.

Future directions

While we now know that serotonin fibers regenerate following traumatic brain injury, there are many questions that these results raise. One is whether serotonin fibers are truly unique in their ability to regenerate following injury. A hypothesis to explain why serotonin fibers are able to regenerate in the neocortex is that the majority of release sites do not have a post-synaptic partner (they utilize volume transmission instead; Beaudet and Descarries, 1978), and therefore regeneration to the same general area may be sufficient to restore function. It is therefore possible that other neuromodulatory systems that do not need to form specific synaptic contacts to exert their influence also retain the ability to regrow in the mature brain. Candidates for this include acetylcholine, dopamine, histamine, and norepinephrine fibers.

Another question raised by the results of the present study is how the serotonin fibers are regrowing. While it has been shown that serotonin fibers can regrow into injured areas both via long distance regeneration and via local sprouting we don't know which dominates here and these processes are indistinguishable in fixed-tissue imaging with

between animal comparisons. Following a penetrating stab injury, *in vivo* imaging revealed that the transected serotonin fibers retract from the stab rift minimally and regrowth occurs from the severed ends into the injured area (Jin et al., 2016). This regeneration is able to regrow through the stab rift despite the presence of a glial scar. Recovery following controlled cortical impact may mirror recovery following a penetrating stab injury. However, because reactive gliosis is much more profound following controlled cortical impact, it is possible that regenerating serotonin fibers are unable to penetrate deep enough into the damaged area and that local sprouting from surviving serotonin accounts for the majority of regrowth. *In vivo* two-photon time-lapse imaging of serotonin fibers following traumatic brain injury would provide the necessary data to address this by allowing for quantification of the rate of local sprouting and visualization of how fibers enter and spread through the injured area.

Similarly, we don't know if all serotonin neurons have the same capacity to regenerate. Results from two-photo *in vivo* imaging of serotonin fiber regeneration following amphetamine lesion showed that serotonin fibers do not regrow in the exact same locations as fibers used to be, suggesting that the original innervation pattern does not need to be replicated for functional recovery (Jin et al., 2016). For instance, if controlled cortical impact leads primarily to the damage of fibers in layer 1 posterior to injury, which originate from the median raphe, do the regrowing fibers originate from same neuronal population, or is layer 1 reinnervated by fibers from the relatively spared dorsal raphe

pathway? Developmentally, all of the dorsal raphe neurons originate from rhombomere 1, while the median raphe contains neurons originating from rhombomeres 1, 2, and 3 (Jensen et al., 2008). It has been recently shown that serotonin neurons have rhombomere lineage-specific gene expression patterns (Okaty et al., 2015). These gene expression patterns are likely to confer subtype-specific functions, which could involve aspects of intrinsic regenerative capacity. Labeling of different serotonin neuron populations would help pinpoint which fibers are most susceptible to damage and which are able to regrow. This would approach could be used to complement the *in vivo* two-photon imaging experiments suggested above.

Could changing the activity of the serotonin system alter serotonin fiber loss following traumatic brain injury or effect regrowth? There is evidence that selective serotonin reuptake inhibitors (SSRIs) expand the recovery window for motor function following stroke in a mouse model by reducing inhibitory interneuron number in premotor cortex (Ng et al., 2015). This finding suggests the serotonin system may itself play a role in mitigating the extent of secondary damage as a result of stroke, and perhaps also traumatic brain injury. It would be interesting, therefore, to see if administration of SSRIs or other serotonin receptor agonists and antagonists could reduce the amount of serotonin fiber loss seen in traumatic brain injury models, or increase the rate or extent of recovery of serotonin fibers. It should be noted, however, that traumatic brain injury leads to a decrease of SERT as well as other serotonin receptors such as 5-HT_{2A}, which are the precise

targets of these proposed treatments (Dam et al., 2007). Treatment timing, therefore, may be critical in revealing an effect.

Lastly, it will be important to confirm that fibers that regrow following traumatic brain injury are functional. While technically difficult, it is possible to measure serotonin release in mouse neocortex using fast-scan cyclic voltammetry (Wood and Hashemi, 2013). This approach was successfully utilized to show that serotonin fibers which regenerated following an amphetamine lesion were in fact competent to release serotonin (Jin et al., 2016).

Conclusion

The studies presented in this dissertation show that serotonin fibers are susceptible to damage from traumatic brain injury, and importantly, that they are able to regrow following this type of insult. This is a big step forward in our understanding of traumatic brain injury as it questions the dogma that there is no significant repair following injury in the mature adult brain. By combining behavioral, biomechanical, biochemical, and physiological data from multiple traumatic brain injury models we can ultimately understand the impact of traumatic brain injury on the serotonin system and help reduce the burden that traumatic brain injury and its clinical sequelae have on the human population.

References

Abe, K., Shimada, R., Okada, Y., and Kibayashi, K. (2016). Traumatic brain injury decreases serotonin transporter expression in the rat cerebrum. Neurological Research **38**. 358-63.

Alilain, W.J., Horn, K.P., Hu, H., Dick, T.E., and Silver, J. (2011). Functional regeneration of respiratory pathways after spinal cord injury. Nature **475**. 196-200.

Beaudet, A. and Descarries, L. (1978). The monoamine innervation of rat cerebral cortex: synaptic and nonsynaptic axon terminals. Neuroscience **3**. 851-60.

Bovolenta, P., Wandosell, F., and Nieto-Sampedro, M. (1993). Characterization of a neurite outgrowth inhibitor expressed after CNS injury. European Journal of Neuroscience **5**. 454-65.

Cantu, D., Walker, K., Andresen, L., Taylor-Weiner, A., Hampton, D., Tesco, G., and Dulla, C.G. (2015). Traumatic Brain Injury Increases Cortical Glutamate Network Activity by Compromising GABAergic Control. Cerebral Cortex **25**. 2306-20.

Canty, A.J., Huang, L., Jackson, J.S., Little, G.E., Knott, G., Maco, B., and De Paola, V. (2013) In-vivo single neuron axotomy triggers axon regeneration to restore synaptic density in specific cortical circuits. Nature Communications **4**. 2038.

Centers of Disease Control and Prevention. (2015). Report to Congress on Traumatic Brain Injury in the United States: Epidemiology and Rehabilitation. National Center for Injury Prevention and Control; Division of Unintentional Injury Prevention. Atlanta, GA.

Chew, D.J., Fawcett, J.W., and Andrews, M.R. (2012). The challenges of long-distance axon regeneration in the injured CNS. Progress in Brain Research **201**. 253-94.

Cho, B.P., Song, D.Y., Sugama, S., Shin, D.H., Shimizu, Y., Kim, S.S., Kim, Y.S., and Joh, T.H. (2006). Pathological dynamics of activated microglia following medial forebrain bundle transection. Glia **53**. 92-102.

Corrigan, J.D., Selassie, A.W., and Orman, J.A. (2010). The epidemiology of traumatic brain injury. Journal of Head Trauma Rehabilitation **25**. 72-80.

Dam, H., Mellerup, E.T., Plenge, P., Winther, R., and Wörtwein, G. (2007). The serotonin transporter and 5HT2A receptor in rat brain after localized lesions. Neurological Research **29**. 717-22.

Davalos, D., Grutzendler, J., Yang, G., Kim, J.V., Zuo, Y., Jung, S., Littman, D.R., Dustin, M.L., and Gan, W.B. (2005). ATP mediates rapid microglial response to local brain injury in vivo. Nature Neuroscience **8**. 752-8.

DeFelipe, J. and Jones, E.G. (1988). A light and electron microscopic study of serotonin-immunoreactive fibers and terminals in the monkey sensory-motor cortex. Experimental Brain Research **71**. 171-82.

Dheen, S.T., Kaur, C., and Ling, E.A. (2007). Microglial activation and its implications in the brain diseases. Current Medicinal Chemistry **14**. 1189-97.

Eng, L.F. and Ghirnikar, R.S. (1994). GFAP and astrogliosis. Brain Pathology **4**. 229-37.

Fakhoury, M. (2016). Revisiting the Serotonin Hypothesis: Implications for Major Depressive Disorders. Molecular Neurobiology **53**. 2778-86.

Faul, M. and Coronado, V. (2015). Epidemiology of traumatic brain injury. Handbook Clinical Neurology **127**. 3-13.

Fedoroff, J.P., Starkstein, S.E., Forrester, A.W., Geisler, F.H., Jorge, R.E., Arndt, S.V., and Robinson, R.G. (1992). Depression in patients with acute traumatic brain injury. American Journal of Psychiatry **149**. 918-23.

Fournier, A.E., GrandPre, T., and Strittmatter, S.M. (2001). Identification of a receptor mediating Nogo-66 inhibition of axonal regeneration. Nature **409**. 341-6.

Fox, G.B., Fan, L., Levasseur, R.A., and Faden, A.I. (1998). Sustained sensory/motor and cognitive deficits with neuronal apoptosis following controlled cortical impact brain injury in the mouse. Journal of Neurotrauma **15**. 599-614.

Hagino, S., Iseki, K., Mori, T., Zhang, Y., Hikake, T., Yokoya, S., Takeuchi, M., Hasimoto, H., Kikuchi, S., and Wanaka, A. (2003). Slit and glypican-1 mRNAs are coexpressed in the reactive astrocytes of the injured adult brain. Glia **42**. 130-8.

Harrison-Felix, C., Whiteneck, G., DeVivo, M., Hammond, F.M., and Jha, A. (2004). Mortality following rehabilitation in the Traumatic Brain Injury Model Systems of Care. NeuroRehabilitation **19**. 45-54.

Hawthorne, A.L., Hu, H., Kundu, B., Steinmetz, M.P., Wylie, C.J., Deneris, E.S., and Silver, J. (2011). The unusual response of serotonergic neurons after CNS Injury: lack of axonal

dieback and enhanced sprouting within the inhibitory environment of the glial scar. Journal of Neuroscience **31**. 5605-16.

Hornung, J.P. (2003). The human raphe nuclei and the serotonergic system. Journal of Chemical Neuroanatomy **26**. 331-43.

Ito, D., Imai, Y., Ohsawa, K., Nakajima, K., Fukuuchi, Y., and Kohsaka, S. (1998). Microglia-specific localisation of a novel calcium binding protein, Iba1. Molecular Brain Research **57**. 1-9.

Jensen, P., Farago, A.F., Awatramani, R.B., Scott, M.M., Deneris, E.S., and Dymecki, S.M. (2008). Redefining the serotonergic system by genetic lineage. Nature Neuroscience **11**. 417-9.

Jin, Y., Dougherty, S.E., Wood, K., Sun, L., Cudmore, R.H., Abdalla, A., Kannan, G., Pletnikov, M., Hashemi, P., and Linden, D.J. (2016). Regrowth of serotonin axons in the adult mouse brain following injury. Neuron, in press.

Jorge, R.E., Robinson, R.G., Moser, D., Tateno, A., Crespo-Facorro, B., and Arndt, S. (2004). Major depression following traumatic brain injury. Archives of General Psychiatry **61**. 42-50.

Kalmbach, A.S. and Waters, J. (2012). Brain surface temperature under a craniotomy. Journal of Neurophysiology **108**. 3138-46.

Kanno, H., Pressman, Y., Moody, A., Berg, R., Muir, E.M., Rogers, J.H., Ozawa, H., Itoi, E., Pearse, D.D., and Bunge, M.B. (2014). Combination of engineered Schwann cell grafts to secrete neurotrophin and chondroitinase promotes axonal regeneration and locomotion after spinal cord injury. Journal of Neuroscience **34**. 1838-55.

Kohler, S., Cierpinsky, K., Kronenberg, G., and Adli, M. (2016). The serotonergic system in the neurobiology of depression: Relevance for novel antidepressants. Journal of Psychopharmacology **30**. 13-22.

Lee, J.K., Chow, R., Xie, F., Chow, S.Y., Tolentino, K.E., and Zheng, B. (2010). Combined genetic attenuation of myelin and semaphorin-mediated growth inhibition is insufficient to promote serotonergic axon regeneration. Journal of Neuroscience **30**. 10899-904.

Lee, Y.S., Lin, C.Y., Jiang, H.H., Depaul, M., Lin, V.W., and Silver, J. (2013). Nerve regeneration restores supraspinal control of bladder function after complete spinal cord injury. Journal of Neuroscience **33**. 10591-606.

Lighthall, J.W., Goshgarian, H.G., and Pinderski, C.R. (1990). Characterization of axonal injury produced by controlled cortical impact. Journal of Neurotrauma **7**. 65-76.

Loane, D.J. and Kumar, A. (2016). Microglia in the TBI brain: The good, the bad, and the dysregulated. Experimental Neurology **275**. 316-27.

Long, J.B., Bentley, T.L., Wessner, K.A., Cerone, C., Sweeney, S., and Bauman, R.A. (2009). Blast overpressure in rats: recreating a battlefield injury in the laboratory. Journal of Neurotrauma **26**. 827-40.

Lucki, I. (1998). The spectrum of behaviors influenced by serotonin. Biological Psychiatry **44**. 151-62.

Manto, M., Gruol, D.L., Schmahmann, J.D., Koibuchi, N., and Rossi, F. (2013). Handbook of the Cerebellum and Cerebellar Disorders. (Springer Netherlands).

Masel, B.E. and DeWitt, D.S. (2010). Traumatic brain injury: a disease process, not an event. Journal of Neurotrauma **27**. 1529-40.

Molliver, M.E., Berger, U.V., Mamounas, L.A., Molliver, D.C., O'Hearn, E., and Wilson, M.A. (1990). Neurotoxicity of MDMA and related compounds: anatomic studies. Annals of the New York Academy of Sciences **600**. 649-61.

Muller, C.P. and Jacobs, B. (2010). Handbook of the Behavioral Neurobiology of Serotonin. (New York: Academic Press).

Murphy, D.L., Andrews, A.M., Wichems, C.H., Li, Q., Tohda, M., and Greenberg, B. (1998). Brain serotonin neurotransmission: an overview and update with an emphasis on serotonin subsystem heterogeneity, multiple receptors, interactions with other neurotransmitter systems, and consequent implications for understanding the actions of serotonergic drugs. Journal of Clinical Psychiatry **59**. 4-12.

Murphy, D.L. and Lesch, K.P. (2008). Targeting the murine serotonin transporter: insights into human neurobiology. Nature Reviews Neuroscience **9**. 85-96.

Nelson, D.L. (2004). 5-HT5 receptors. Current Drug Targets - CNS & Neurological Disorders **3**. 53-8.

Ng, K.L., Gibson, E.M., Hubbard, R., Yang, J., Caffo, B., O'Brien, R.J., Krakauer, J.W., and Zeiler, S.R. (2015). Fluoxetine Maintains a State of Heightened Responsiveness to Motor Training Early After Stroke in a Mouse Model. Stroke **46**. 2951-60.

Ohtake, Y. and Li, S. (2015). Molecular mechanisms of scar-sourced axon growth inhibitors. Brain Research **1619**. 22-35.

Okaty, B.W., Freret, M.E., Rood, B.D., Brust, R.D., Hennessy, M.L., deBairos, D., Kim, J.C., Cook, M.N., and Dymecki, S.M. (2015). Multi-Scale Molecular Deconstruction of the Serotonin Neuron System. Neuron **88**. 774-91.

Ridler, T.W. and Calvard, S. (1978). Picture thresholding using an iterative selection method. IEEE Transactions on Systems, Man, and Cybernetics **8**. 630-2.

Riggio, S. and Wong, M. (2009). Neurobehavioral sequelae of traumatic brain injury. Mount Sinai Journal of Medicine **76**. 163-72.

Scheib, J. and Hoke, A. (2013). Advances in peripheral nerve regeneration. Nature Reviews Neurology **9**. 668-76.

Silver, J.M., McAllister, T.W., and Arciniegas, D.B. (2009). Depression and cognitive complaints following mild traumatic brain injury. American Journal of Psychiatry **166**. 653-61.

Smith, D.H., Soares, H.D., Pierce, J.S., Perlman, K.G., Saatman, K.E., Meaney, D.F., Dixon, C.E., and McIntosh, T.K. (1995). A model of parasagittal controlled cortical impact in the mouse: cognitive and histopathologic effects. Journal of Neurotrauma **12**. 169-78.

Smith, D.H., Chen, X.H., Pierce, J.E., Wolf, J.A., Trojanowski, J.Q., Graham, D.I., and McIntosh, T.K. (1997). Progressive atrophy and neuron death for one year following brain trauma in the rat. Journal of Neurotrauma **14**. 715-27.

Sofroniew, M.V. (2009). Molecular dissection of reactive astrogliosis and glial scar formation. Trends in Neurosciences **32**. 638-47.

Sun, F. and He, Z. (2010). Neuronal intrinsic barriers for axon regeneration in the adult CNS. Current Opinion in Neurobiology **20**. 510-8.

Szalay, G., Martinecz, B., Lénárt, N., Környei, Z., Orsolits, B., Judák, L., Császár, E., Fekete, R., West, B.L., Katona, G., Rózsa, B., and Dénes, Á. (2016). Microglia protect against brain

injury and their selective elimination dysregulates neuronal network activity after stroke. Nature Communications **7**. 11499.

Tork, I. (1990). Anatomy of the serotonergic system. Annals of the New York Academy of Sciences **600**. 9-34.

Tsai, H.C., Zhang, F., Adamantidis, A., Stuber, G.D., Bonci, A., de Lecea, L., and Deisseroth, K. (2009). Phasic firing in dopaminergic neurons is sufficient for behavioral conditioning. Science **324**. 1080-4.

Tuszynski, M.H. and Steward, O. (2012). Concepts and methods for the study of axonal regeneration in the CNS. Neuron **74**. 777-91.

Vitalis, T., Ansorge, M.S., and Dayer, A.G. (2013). Serotonin homeostasis and serotonin receptors as actors of cortical construction: special attention to the 5-HT3A and 5-HT6 receptor subtypes. Frontiers in Cellular Neuroscience **7**. 93.

Williams, W.H., Potter, S., and Ryland, H. (2010). Mild traumatic brain injury and Postconcussion Syndrome: a neuropsychological perspective. Journal of Neurology, Neurosurgery & Psychiatry **81**. 1116-22.

Wilson, M.A. and Molliver, M.E. (1994). Microglial response to degeneration of serotonergic axon terminals. Glia **11**. 18-34.

Wood, K.M. and Hashemi, P. (2013). Fast-scan cyclic voltammetry analysis of dynamic serotonin reponses to acute escitalopram. ACS Chemical Neuroscience **4**. 715-20.

Xiong, Y., Mahmood, A., and Chopp, M. (2013). Animal models of traumatic brain injury. Nature Reviews Neuroscience **14**. 128-42.

Xu, L., Nguyen, J.V., Lehar, M., Menon, A., Rha, E., Arena, J., Ryu, J., Marsh-Armstrong, N., Marmarou, C.R., and Koliatsos, V.E. (2016). Repetitive mild traumatic brain injury with impact acceleration in the mouse: Multifocal axonopathy, neuroinflammation, and neurodegeneration in the visual system. Experimental Neurology **275**. 436-49.

Yiu, G. and He, Z. (2006). Glial inhibition of CNS axon regeneration. Nature Reviews Neuroscience **7**. 617-27.

Yoo, M., Khaled, M., Gibbs, K.M., Kim, J., Kowalewski, B., Dierks, T., and Schachner, M. (2013). Arylsulfatase B improves locomotor function after mouse spinal cord injury. PLoS One **8**. e57415.

Yu, S., Kaneko, Y., Bae, E., Stahl, C.E., Wang, Y., van Loveren, H., Sanberg, P.R., and Borlongan, C.V. (2009). Severity of controlled cortical impact traumatic brain injury in rats and mice dictates degree of behavioral deficits. Brain Research **1287**. 157-63.

Zou, H., Ho, C., Wong, K., and Tessier-Lavigne, M. (2009). Axotomy-induced Smad1 activation promotes axonal growth in adult sensory neurons. Journal of Neuroscience **29**. 7116-23.

Curriculum Vitae

Tymoteusz Jan Kajstura

Education

2007 B.A, Neuroscience/Biology, Oberlin College, OH
2016 Ph.D., Neuroscience, Johns Hopkins School of Medicine, MD

Awards

2006 Goldwater Scholarship

Research Publications

Laskowski M, Biller S, Stanley K, **Kajstura T**, Prusty R. Expression Profiling of Auxin-Treated *Arabidopsis* Roots: Toward a molecular analysis of lateral root emergence. Plant Cell Physiol., 2006 Jun;47(6):788-92.

Rota M, Boni A, Urbanek K, Padin-Iruegas E, **Kajstura T**, Fiore G, Kudo H, Sonnenblick E, Musso E, Houser S, Leri A, Sussman M, Anversa P. Nuclear Targeting of Akt Enhances Ventricular Function and Myocyte Contractility. Circ Res., 2005 Dec 9;97(12):1332-41.

Research Presentations

Shevelkin AV, Abazyan BN, Yang C, Mychko OA, **Kajstura TJ**, Troncoso JC, Linden DJ, Pletnikov MV. Autism-like Neurobehavioral Abnormalities in Mice with Selective Expression of Mutant DISC1 in Purkinje Cells of the Anterior Cerebellum. Biol. Psychiatry, 2016 May 1;79(9, Suppl.):60S.

Rizzi R, Arcarese ML, Esposito G, Bearzi C, Korn JA, Di Marco A, **Kajstura TJ**, Hosoda T, Steadman E, Urbanek K, D'Amario D, Sonnenblick EH, Leri A, Anversa P, Rota M. Intracellular calcium cycling mediates proliferation and differentiation of human cardiac stem cells. Circulation, 2007 Oct 16;116(16, Suppl.):203.

Rota M, De Angelis A, Urbanek K, Musso E, Iaffaldano G, **Kajstura TJ**, Mosna F, Gatti A, Valentini S, Delucchi F, Mitchell TS, Leri A, Sonnenblick EH, Anversa P. Myocyte Aging Conditions Cell Growth and Contractile Function. Circulation, 2006 Oct 31;114(18, Suppl.):279.

Rota M, De Angelis A, Tillmanns J, Mitchell TS, Musso E, Urbanek K, Iaffaldano G, Esposito G, **Kajstura TJ**, Misao Y, Miqueo AG, Rotatori F, Leri A, Sonnenblick EH, Bolli R, Anversa P. Cardiac Stem Cells Regenerate the Coronary Vasculature and the Scarred Infarcted Myocardium in Rats. Circulation, 2006 Oct 31;114(18, Suppl.):265.

Laskowski MJ, Condon B, **Kajstura TJ**. In Search of a Molecular Houdini: Do Pectate Lyases Allow Lateral Roots to Emerge? American Society of Plant Biologists, Boston, MA, 2006. Epub only.

Rota M, Boni A, Urbanek K, Musso E, **Kajstura T**, Whang B, Coku L, Fiore G, Liu R, Anversa P, Sonnenblick E, Sussman M, Leri A. Targeted Overexpression of Akt in Myocyte Nuclei Promotes Cell Regeneration and Enhances Myocyte Mechanical Performance. Circulation, 2005 Oct 25;112(17, Suppl.):U197.

Nascimbene A, Casarsa C, Boni A, Sheikh F, Hosoda T, Fiumana E, Valentini S, **Kajstura T**, Amano K, Zias E, Anversa P, Bolli R, Leri A. The Cell Fate Determinant Notch Maintains Cardiac Progenitor Cells in an Undifferentiated State. Circulation, 2005 Oct 25;112(17, Suppl.):U206.